Chaos

Influence of higher-order modes on ferroconvection

Cite as: Chaos **32**, 083129 (2022); https://doi.org/10.1063/5.0097398
Submitted: 28 April 2022 • Accepted: 21 July 2022 • Published Online: 16 August 2022

C. Kanchana, J. A. Vélez, L. M. Pérez, et al.

COLLECTIONS

This paper was selected as an Editor's Pick

View Online Export Citation CrossMark

APL Machine Learning
Open, quality research for the networking communities
Now Open for Submissions
LEARN MORE

AIP Publishing

© 2022 Author(s).

Influence of higher-order modes on ferroconvection

Cite as: Chaos **32**, 083129 (2022); doi: 10.1063/5.0097398
Submitted: 28 April 2022 · Accepted: 21 July 2022 ·
Published Online: 16 August 2022

View Online Export Citation CrossMark

C. Kanchana,[1,a)] J. A. Vélez,[2] L. M. Pérez,[3] D. Laroze,[2] and P. G. Siddheshwar[4]

AFFILIATIONS

[1]Instituto de Alta Investigación, Sede Esmeralda, Universidad de Tarapacá, Av. Luis Emilio Recabarren 2477, Iquique, Chile
[2]Instituto de Alta Investigación, CEDENNA, Universidad de Tarapacá, Casilla 7 D, Arica 1000000, Chile
[3]Departamento de Física, FACI, Universidad de Tarapacá, Casilla 7 D, Arica 1000000, Chile
[4]Center for Mathematical Needs, Department of Mathematics, CHRIST(Deemed to be University), Bengaluru 560029, India

[a)]**Author to whom correspondence should be addressed:** ckanchana@academicos.uta.cl

ABSTRACT

Using Fourier representations, an elaborate study of regular cellular-convective and chaotic motions in a ferrofluid is made. Investigation is made on the adequacy or otherwise of the minimal mode in studying such motions. Higher-order modes are also considered by adding modes (vertical/horizontal/combined extension). For higher modes, the extensions yield a dynamical system of order greater than three. The characteristic features of extended ferromagnetic-Lorenz models are analyzed using the largest Lyapunov exponent(LE), second largest LE, bifurcation diagram, and phase-space plots. The effect of additional modes on critical modal-Rayleigh (infinitesimal and finite-amplitude ones) numbers and the Rayleigh number at which transition to chaos occurs are examined to report features of ferroconvection hitherto unseen in previous studies. As both horizontal and vertical modes are increased, our findings infer that the dynamical system displays advanced onset of regular convection and delayed chaotic motion. Vigorous-chaotic motion is seen on adding vertical modes, whereas on adding horizontal modes, intense chaos appears with decreased intensity for large values of the scaled Rayleigh number. Most important finding from the study is that as modes are increased (vertical/horizontal), the transition from regular to chaotic motion is greatly modified and leads the system to a hyper-chaotic state. Conventionally, the chaotic or hyper-chaotic state is intermittent with a periodic/quasi-periodic state but it can be retained in the chaotic or hyper-chaotic state by considering moderate values of the Prandtl number and/or by bringing in the ferromagnetic effect.

Published under an exclusive license by AIP Publishing. https://doi.org/10.1063/5.0097398

Vertical and/or horizontal extensions of a minimal Fourier mode lead to generalized Lorenz models of ferroconvection of order greater than three. In such systems, there is a possibility of regular cellular motion, chaotic motion as well as hyper-chaos. Hyper chaos can be observed in these systems in the case of low Prandtl number fluids and high Rayleigh numbers whereas chaos is preferred in high Prandtl number ones at low Rayleigh number values. Further, a magnetic field of appropriate strength can be effectively used in retaining either chaotic or hyper-chaotic systems.

I. INTRODUCTION

Two important fluids that have been in the limelight, of late, are nanofluids and ferrofluids. The nanofluids have nanoparticles well-dispersed in a carrier fluid,[1–5] whereas ferrofluids have micrometer or sub-micrometer-sized particles in a carrier fluid in a way similar to nano ones. The impossibility of using micrometer-sized particles (with better thermal conductivity than the carrier fluid) due to agglomeration, abrasiveness, and other dissuading factors led people to think of coating of these particles. The ferrofluid is one such example wherein a ferrite particle is coated with oleic acid to prevent agglomeration, settling, and abrasiveness.[6–8] The external magnetic field applied on the system served the purpose of regulation of flow through a strong influence by the magnetic field on the thermorheological and magnetorheological properties. This new suggestion for a fluid-based system did not take off to the extent that the scientists wished for due to the fact that the regulation mechanism involved an applied magnetic field. With technology improving vastly in the last two decades, the world saw miniaturization of particles beyond the micrometer-sized ones. At the present

time, engineers have succeeded in manufacturing nano-sized particles of uniform shape and size together with uniform thermal and magnetic properties. A wide variety of nanoparticles have been on the scene in the recent past with one very attractive feature in them being their higher thermal conductivity when compared with that of the carrier fluid in which they are suspended. Preliminary experiments showed that with a dilute concentration of nanoparticles (less than 6%), it is possible to have an "enhanced heat transfer" situation. With the above observation, it thus becomes clear that ferrofluids serve situations involving control of a thermal environment through the regulation of thermorheological properties and nanofluids serve thermal cooling applications without the need to control thermorheological properties. In the former, the residence time of heat can be controlled, whereas in the latter, it is decreased and this depends on the volume fraction of the nanoparticles. With our focus being on heat transfer and its regulation, we concentrate only on ferrofluids. A class of micrometer-sized particles called magnetic particles are those particles that show response to an applied magnetic field. These particles are classified into the following five types based on their behavior: ferromagnetic, paramagnetic, diamagnetic, antiferromagnetic, and ferrimagnetic. In ferromagnetic materials, an atom has a net magnetic moment due to unpaired electrons. When the ferromagnetic particle is placed in a magnetic field, the magnetic moments of the domains align along the direction of the applied magnetic field forming a large net magnetic moment. Materials such as iron, nickel, and cobalt belong to the family of ferromagnetic particles. A carrier fluid in which are present well-dispersed ferromagnetic particles is called a ferrofluid (or a ferromagnetic fluid). The suspended ferro-magnetic particles in a carrier fluid have the tendency of agglomeration and this can be avoided by coating these particles with a surfactant like oleic acid, soy lecithin, and citric acid. Due to the surfactant-coated particles, the ferrofluids become highly stable and have strong magnetic properties. Ferrofluid has a wide range of applications in various fields. In medicine, it is used to transport drugs to an injured part of the body and in the removal of tumors from the body. Ferrofluid is used as a coolant in rotating shaft seals, loudspeaker, printers and as semi-active dampers in mechanical and aerospace applications. Ferrofluids are naturally used in heat transfer applications including thermomagnetic convection. Due to the presence of ferromagnetic particles, the carrier fluids exhibit drastic enhancement in their thermal conductivity thereby leading to an enhancement in heat transport. Ferrofluids are called as "smart fluids" since their dynamics can be rheologically controlled through an external means of an applied magnetic field.[8]

The synthesize of a ferrofluid was for the first time made by Rosensweig[6,9,10] and, in fact, the prefix "ferro" was given by him. A comprehensive linear stability analysis of Rayleigh–Bénard convection (RBC) in a ferrofluid was reported by Finlayson[11] considering both magnetic and buoyancy mechanisms. Importance of these two mechanisms and parameter ranges at which these two mechanisms exist or are rendered unimportant were explained in detail in the paper using the concept of a new parameter called the magnetic-Rayleigh number. After this work,[11] RBC in ferrofluids came to be called as *ferroconvection* and we too use the terminology. The results of Finlayson[11] were subsequently examined theoretically by Schwab *et al.*[12] and experimentally by Stiles and Kagan.[13] Blennerhassett *et al.*[14] showed that under microgravity conditions, ferrofluid facilitates heat transport enhancement upto 10% in the presence of a strong magnetic field. Sekhar *et al.*[15] studied influence of different boundary combinations (rigid–rigid, rigid–free, and free–free) and internal heat generation on onset of ferroconvection and concluded that the rigid–rigid boundary condition is the most stable configuration than the remaining two. Lalas and Carmi[16] reported that the linear stability and the energy stability provide identical results for stationary ferromagnetic convection. Gupta and Gupta[17] studied the onset of regular convection in a horizontal ferromagnetic fluid layer rotating about a vertical axis in the presence of a uniform magnetic field. Influence of rotation on the onset of ferroconvection was highlighted in the paper. Influence of second sound on linear stability of ferroconvection was investigated by Siddheshwar[18] by transiting from the classical Fourier law to a non-Fourier law of the Maxwell–Cattaneo type. Siddheshwar[19] also extended the problem of ferroconvection using general boundary conditions on the velocity, the temperature, and the scalar magnetic potential and reaffirmed the qualitative findings of previous investigators in limiting cases. Bajaj and Malik[20,21] studied the pattern formation in a ferrofluid and showed that rolls are more stable than square and hexagonal lattices.

We now cover the works of ferroconvection in the last decade. Ferromagnetic convection in the presence of body force was studied by Siddheshwar and Annamma[22] and under hypergravity and microgravity it was studied by Chong *et al.*[23] Comparison of the results of energy stability with those of linear and weakly nonlinear stabilities was included by Straughan[24] in his book. Sunil and Mahajan[25] made similar comparison by varying the magnetic parameters, and then Siddheshwar *et al.*[26] made a further extension by including, in addition, linear and weakly nonlinear stability analyses. Effects of the relaxation time and the rotational viscosity on ferroconvection were made by Kaloni and Lou.[27] Thermomagnetic convection in a vertical ferrofluid layer was investigated by Suslov,[28] and Dey and Suslov.[29] The influence of internal heat generation on the energy stability of a ferrofluid layer was reported by Mahajan and Sharma.[30] Nonlinear study of rotating ferroconvection in a porous layer was undertaken by Mahajan and Parashar,[31] while Melson *et al.*[32] studied the same problem without a porous matrix. Other studies on ferroconvection can be found in Refs. 33–41.

The chaotic motion in dynamical systems of RBC was reported for the first time by Lorenz.[42] Using the argument of Lorenz, there have been many reported works on chaotic motion.[43–56] Bozhko and Putin[57] examined influence of an external, homogeneous magnetic field (transversal/longitudinal) on ferroconvection in horizontal, inclined, and vertical layers. They noticed spiral-defect chaos, blinking and localized states. Using mathematical tools like Fourier power spectrum, bifurcation diagrams, and Lyapunov exponents, Laroze *et al.*[58] studied chaotic behavior in the tri-modal ferromagnetic-Lorenz model. The discussion made so far on the dynamical system (called the Lorenz model) is associated with the hydrodynamics aspect. However, the Lorenz model is also associated with some general instabilities.[59] The detailed literature survey on the latter aspect is excluded in the paper.

In the present paper, we study the regular cellular -convective motion and chaotic motion in the ferroconvective system by extending modes of Fourier spectrum horizontally, vertically, and then simultaneously increasing horizontal and vertical modes. The

Published under an exclusive license by AIP Publishing

Fourier spectrum reported by Saltzman[60] is used in the study to derive extended-ferromagnetic-Lorenz models. The works by Roy and his team,[61,62] Musielak *et al.*,[63] Musielak and Musielak[64] and Shen[65] are used as guidelines. In the present paper, the study of linear and weakly nonlinear stability analyses of ferroconvection is made in a most general way. In this sense, the present study is a major deviation from reported works on ferroconvection. Using extended-ferromagnetic-Lorenz models furthermore, the symmetric and the Hamiltonian nature of the dynamical systems are explained. The other novelties in the paper include:

(i) Deriving an explicit analytical expression for the modal-Rayleigh number facilitating the study of the influence of each considered mode on the stability of ferroconvection,
(ii) Proving that sub-critical motion is possible (using the minimal truncated Fourier series representation),
(iii) Showing that an analytical expression of the Hopf–Rayleigh number can be obtained,
(iv) Ascertaining whether mildly chaotic/nearly periodic motion is real or is a consequence of severe truncation,
(v) Making a detailed investigation on the influence of higher modes on chaotic ferroconvection,
(vi) Exploring the possibility of hyper-chaos in the higher-order dynamical system, and
(vii) Extracting the influence of the Prandtl number (representing the working medium) and the ferromagnetic effect on the chaotic/hyper-chaotic regimes of the dynamics.

In order to study the aforementioned novelties, the paper is organized as follows. The mathematical formulation in Sec. II includes governing equations, boundary conditions, solution of the conduction and perturbation states, non-dimensionalization, the Fourier spectral method, linear and weakly nonlinear stability analyses, derivation of minimal-mode and extended-mode ferromagnetic-Lorenz models and features of these models. In Sec. III, the results and discussion pertaining to the onset of regular convective motion and chaotic motion are presented. Finally, the conclusion from the study is reported in Sec. IV.

II. MATHEMATICAL FORMULATION

Figure 1 is the schematic of a RBC setup in a smart fluid (ferrofluid) of infinite horizontal extent and thickness h. The upper and lower boundaries are held at constant temperatures T_0 and $T_0 + \Delta T(\Delta T > 0)$, respectively. The governing equations for the proposed problem are the following system of nonlinear partial differential equations (initial-boundary value problem):

$$\nabla \cdot \vec{v} = 0, \tag{1}$$

$$\rho_0 \frac{d\vec{v}}{dt} = -\nabla p + \rho_0 \left[1 - \alpha(T - T_0)\right]\vec{g} + \mu\nabla^2\vec{v} + \nabla\cdot(\vec{H}\vec{B}), \tag{2}$$

$$\left[\rho C_{VH} - \mu_0 H \cdot \left(\frac{\partial M}{\partial T}\right)_{V,H}\right]\frac{dT}{dt} + \mu_0 T\left(\frac{\partial M}{\partial T}\right)_{V,H}\cdot\frac{dH}{dt} = k\nabla^2 T, \tag{3}$$

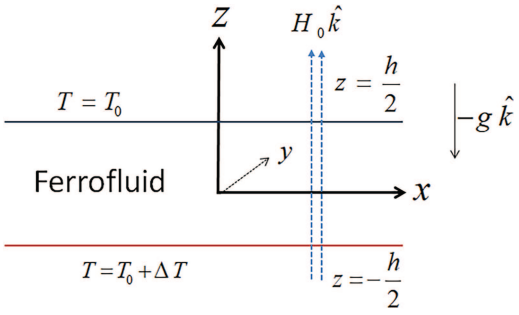


FIG. 1. Physical configuration.

where $\vec{v}$ is the fluid velocity in m/s, ρ_0 is the density in kg/m at the temperature T_0, t is the time in s, p is the pressure in Pa, α is the thermal expansion coefficient in 1/K, $\vec{g}$ is the acceleration due to gravity in m/s^2 , μ is the fluid dynamic viscosity in kg/m s, $\vec{H}$ is the magnetic field, $\vec{B}$ is the magnetic induction, C_{VH} is the heat capacity at constant volume and magnetic field, T is the temperature in K, and k is the thermal conductivity of the fluid in W/m K.

In writing Eq. (2), we have assumed that the viscosity is independent of the temperature and the magnetic field and hence it is isotropic.[6] Furthermore, we have considered the Oberbeck–Boussinesq approximation.[66] The ferrofluid is electrically non-conducting. Maxwell equations for the magnetic field, $\vec{H}$, and the magnetic induction, $\vec{B}$ are given by

$$\nabla \times \vec{H} = 0, \quad \nabla \cdot \vec{B} = 0. \tag{4}$$

From the equation $\nabla \times \vec{H} = 0$, we can write $\vec{H} = \nabla\phi$, where ϕ is the magnetic potential. The relationship between these fields is

$$\vec{B} \equiv \mu_0(\vec{H} + \vec{M}), \tag{5}$$

where μ_0 is the magnetic permeability and $\vec{M} = M(T,H)\hat{H}$ is the magnetization.

The magnetic equation of state is given by Finlayson[11]

$$M(T,H) = M_0 - K(T - T_0) + \chi(H - H_0), \tag{6}$$

where K and χ are the pyromagnetic and magnetic susceptibility coefficients, respectively, and are given by

$$K \equiv -\left(\frac{\partial M}{\partial T}\right)_{H_0,T_0} \text{ and } \chi \equiv \left(\frac{\partial M}{\partial H}\right)_{H_0,T_0}. \tag{7}$$

The variable, $M_0 = M(T_0, H_0)$, is the reference magnetization and $H_0\hat{k}$ is the applied, uniform, vertical magnetic field. We assume for Eqs. (1) and (2) the velocity boundary condition, $\vec{v} = 0$, and the temperature is assumed constant at top and bottom planes,

$$\left.\begin{aligned} T = T_0 + \Delta T \text{ at } z = -\frac{h}{2} \\ T = T_0 \text{ at } z = \frac{h}{2} \end{aligned}\right\}. \tag{8}$$

Published under an exclusive license by AIP Publishing

In the quiescent basic state, the solution of (2) and (3) and (6), subject to Eq. (8), is written as

$$\left.\begin{aligned}\vec{v}=0,\ T_b=\frac{1}{2}(T_0+T_1)-\beta z,\ \beta=\frac{\Delta T}{d},\\ \vec{H}_0=\left(H_0-\frac{K\beta z}{1+\chi}\right)\hat{\mathbf{k}},\ \vec{M}_0=\left(M_0+\frac{K\beta z}{1+\chi}\right)\hat{\mathbf{k}}\end{aligned}\right\}. \tag{9}$$

Considering a perturbation of the basic state and using the following characteristic scales: h for length, h^2/κ for time, κ/h for velocity, βh for temperature, $T_0h^2K/(1+\chi)$ for magnetic scalar potential, and $\mu k/h^2$ for pressure, we obtain

$$\nabla\cdot\vec{v}=0, \tag{10}$$

$$\frac{1}{Pr}\frac{\partial\vec{v}}{\partial t}=-\nabla p_{eff}+Ra(1+M_1)\theta\hat{k}-RaM_1\phi_z\hat{\mathbf{k}}+\nabla^2\vec{v} - RaM_1\theta\nabla\phi_z, \tag{11}$$

$$\frac{\partial\theta}{\partial t}+(\vec{v}\cdot\nabla)\theta-M_2\theta\frac{\partial D\phi}{\partial t}=\nabla^2\theta+(1-M_2)w, \tag{12}$$

$$M_3\frac{\partial^2\phi}{\partial x^2}+\frac{\partial^2\phi}{\partial z^2}-\frac{\partial\theta}{\partial z}=0, \tag{13}$$

where $\vec{v},\theta$, and ϕ, respectively, represent the non-dimensional velocity, temperature, and the magnetic potential. The non-dimensional numbers are defined as

$$p_{eff}=p-\frac{\mu_0M_0}{2H_0}\phi_x^2-\frac{\mu_0\chi}{2}\phi_z^2,\ \text{(effective pressure)}$$

$$M_1=\frac{\mu_0K^2\Delta T}{\rho_0g(1+\chi)h}\ \text{(ratio of the magnetic and the buoyancy forces)},$$

$$M_2=\frac{\mu_0K^2\Delta T}{\rho_0C(1+\chi)}\ \text{(non-buoyancy magnetization parameter)},$$

$$M_3=\frac{H_0+M_0}{H_0(1+\chi)}\ \text{(buoyancy magnetization parameter)},$$

$$Pr=\frac{\mu}{\rho_0\kappa}\text{(Prandtl number)},$$

$$Ra=\frac{\rho_0\alpha\Delta Th^3g}{\mu\kappa}\ \text{(Rayleigh number)}.$$

In writing Eq. (11), we have assumed small scale convective motion. By applying curl twice to Eq. (11) and considering the z-component, we obtain

$$\frac{1}{Pr}\frac{\partial}{\partial t}(\nabla^2w)=\nabla^4w+Ra(1+M_1)\frac{\partial^2\theta}{\partial x^2}-RaM_1\frac{\partial^2\phi_z}{\partial x^2} - RaM_1\frac{\partial}{\partial x}J(\theta,\phi_z), \tag{14}$$

where $J(\theta,\phi_z)$ represents the Jacobian term and is defined as

$$J(\theta,\phi_z)=\frac{\partial\theta}{\partial x}\frac{\partial\phi_z}{\partial z}-\frac{\partial\theta}{\partial z}\frac{\partial\phi_z}{\partial x}. \tag{15}$$

Since M_2 is of order 10^{-6}, in writing Eq. (14) we neglect the term having M_2 as done by Finlayson.[11] The system of Eqs. (10), (12), and (13) are now written in a component form as

$$\frac{\partial u}{\partial x}+\frac{\partial w}{\partial z}=0, \tag{16}$$

$$\frac{\partial\theta}{\partial t}+\left(u\frac{\partial\theta}{\partial x}+w\frac{\partial\theta}{\partial z}\right)=\nabla^2\theta+w, \tag{17}$$

$$M_3\frac{\partial^2\phi}{\partial x^2}+\frac{\partial^2\phi}{\partial z^2}-\frac{\partial\theta}{\partial z}=0. \tag{18}$$

We now define the stream function in the following way so that Eq. (16) is satisfied,

$$u=-\frac{\partial\psi}{\partial z},\ w=\frac{\partial\psi}{\partial x}. \tag{19}$$

Equations (14), (17), and (18) can now be represented in terms of the stream function as follows:

$$\frac{1}{Pr}\frac{\partial}{\partial t}\left(\frac{\partial}{\partial x}(\nabla^2\psi)\right)=\frac{\partial}{\partial x}(\nabla^4\psi)+Ra(1+M_1)\frac{\partial^2\theta}{\partial x^2} - RaM_1\frac{\partial^2\phi_z}{\partial x^2}-RaM_1\frac{\partial}{\partial x}J(\theta,\phi_z), \tag{20}$$

$$\frac{\partial\theta}{\partial t}=\nabla^2\theta+\frac{\partial\psi}{\partial x}+J(\psi,\theta), \tag{21}$$

$$M_3\frac{\partial^2\phi}{\partial x^2}+\frac{\partial^2\phi}{\partial z^2}-\frac{\partial\theta}{\partial z}=0, \tag{22}$$

where

$$J(\psi,\theta)=\frac{\partial\psi}{\partial z}\frac{\partial\theta}{\partial x}-\frac{\partial\psi}{\partial x}\frac{\partial\theta}{\partial z}. \tag{23}$$

The system of Eqs. (20)–(22) are solved subject to the following boundary condition in a non-dimensional form,

$$\psi=\frac{\partial^2\psi}{\partial z^2}=\theta=\frac{\partial\phi}{\partial z}=0\ \text{at}\ z=0,1. \tag{24}$$

A. Fourier spectral method

By following the work of Saltzman,[60] we now consider the following double-Fourier series solution for velocity, temperature, and viscous dissipation having fundamental wavelength, l, in the x-direction and $2h$ in the z-direction,

$$\psi(x,z,t)=\frac{\sqrt{2}}{\pi}\sum_{m=-\infty}^{\infty}\sum_{n=-\infty}^{\infty}\delta_{m,n}^2\psi(m,n,t) \times\exp\left\{i\left[2m\pi\left(\frac{h}{l}\right)x+n\pi z\right]\right\}, \tag{25}$$

$$\theta(x,z,t)=\frac{1}{\pi}\sum_{m=-\infty}^{\infty}\sum_{n=-\infty}^{\infty}\theta(m,n,t) \times\exp\left\{i\left[2m\pi\left(\frac{h}{l}\right)x+n\pi z\right]\right\}, \tag{26}$$

Published under an exclusive license by AIP Publishing

$$\phi(x,z,t) = \frac{1}{\pi}\sum_{m=-\infty}^{\infty}\sum_{n=-\infty}^{\infty}\phi(m,n,t) \times \exp\left\{i\left[2m\pi\left(\frac{h}{l}\right)x + n\pi z\right]\right\}, \quad (27)$$

where m and n are the modes in the x and z directions, $\delta^2_{m,n} = \pi^2[(2m-1)^2q^2 + (2n-1)^2]$ and $q = h/l$ is the wave number. The terms, $\psi(m,n,t)$, $\theta(m,n,t)$ and $\phi(m,n,t)$, are the complex Fourier coefficients given by

$$\Psi_{m,n}(t) = \frac{\delta^2_{m,n}}{\sqrt{2}\pi lh}\int_0^l\int_{-h}^h \psi(x,z,t) \times \exp\left\{-i\left[2m\pi\left(\frac{h}{l}\right)x + n\pi z\right]\right\} dx\,dz, \quad (28)$$

$$\Theta_{m,n}(t) = \frac{1}{2\pi lh}\int_0^l\int_{-h}^h \theta(x,z,t) \times \exp\left\{-i\left[2m\pi\left(\frac{h}{l}\right)x + n\pi z\right]\right\} dx\,dz, \quad (29)$$

$$\Phi_{m,n}(t) = \frac{1}{2\pi lh}\int_0^l\int_{-h}^h \phi(x,z,t) \times \exp\left\{-i\left[2m\pi\left(\frac{h}{l}\right)x + n\pi z\right]\right\} dx\,dz. \quad (30)$$

Substituting Eqs. (25)–(27) into the governing Eqs. (20)–(22) and integrating over one wavelength, we obtain the set of ordinary differential equations in terms of $\Psi_{m,n}(t)$, $\Theta_{m,n}(t)$, and $\Phi_{m,n}(t)$. By adopting the approach of Saltzman,[60] we express $\Psi_{m,n}(t)$, $\Theta_{m,n}(t)$, and $\Phi_{m,n}(t)$ in terms of their real and imaginary parts as follows:

$$\left.\begin{aligned}\Psi_{m,n} &= \Psi_{1\,m,n} - i\Psi_{2m,n}\\ \Theta m,n &= \Theta_{1\,m,n} - i\Theta_{2m,n}\\ \Phi_{m,n} &= \Phi_{1\,m,n} - i\Phi_{2m,n}\end{aligned}\right\}. \quad (31)$$

For cellular-convective motions, the modes pertaining to $\Psi_{2m,n}$, $\Theta_{1\,m,n}$, and $\Phi_{2m,n}$ are excluded for further computation[60] and using Eq. (22), we obtain

$$\left.\begin{aligned}\Phi_{1\,m,n} &= -\frac{\pi(2n-1)}{\eta^2_{m,n}}\Theta_{2(m,n)},\\ \Phi_{1(0,2n)} &= -\frac{1}{2n\pi}\Theta_{2(0,2n)}\end{aligned}\right\} \text{ for } m>0, n>0, \quad (32)$$

where $\eta^2_{m,n} = \pi^2[M_3(2m-1)^2q^2 + (2n-1)]$.

B. Linear stability analysis

To perform a linear stability analysis of ferroconvection, we consider the following modes:

$\Psi_{1\,m,n}$: which describes the convective cells and
$\Theta_{2m,n}$: which describes the horizontal temperature difference in the convective cells.

Substituting the Fourier spectrum of Eqs. (25)–(27) in the linearized, steady state version of the governing Eqs. (20)–(22) and using Eq. (32) and the orthogonality condition, we get a homogeneous system of equations in terms of Ψ_1 and Θ_2. The condition for the occurrence of a non-trivial solution of the homogeneous system is

$$\begin{vmatrix}\delta^4_{m,n} & -\pi q(2m-1)\xi_{m,n}Ra\\ \pi q(2m-1) & -\delta^2_{m,n}\end{vmatrix} = 0, \quad (33)$$

where $\xi_{m,n} = \dfrac{\eta^2_{m,n}(1+M_1) - M_1(2n-1)^2\pi^2}{\eta^2_{m,n}}$.

Solving Eq. (33), we get the following expression for Ra (hereafter we refer to Ra as $Ra_{m,n}$, a modal Rayleigh number):

$$Ra_{m,n} = \frac{\delta^6_{m,n}}{\pi^2q^2(2m-1)^2\xi_{m,n}}. \quad (34)$$

Minimizing the above expression with respect to q, we get the critical Rayleigh and the wave numbers for different modes. Equation (34) involves M_1 and M_3. When $M_1 = 0$, we get the expression of the classical Rayleigh number.[67] For large values of M_1, we obtain an expression for the modal-magnetic Rayleigh number, $R_{m,n}$, from Eq. (34),

$$R_{m,n} = \frac{\delta^6_{m,n}\eta^2_{m,n}}{\pi^4q^4(2m-1)^4M_3}. \quad (35)$$

This expression for the modal-magnetic Rayleigh number is identical to the expressions obtained by Finlayson[11] and Laroze *et al.*[58]

C. Weakly nonlinear stability analysis

To perform a weakly nonlinear stability analysis, we consider the modes mentioned in the linear theory and additional modes pertaining to a change in the horizontal mean and thus, we have

$\Psi_{1\,m,n}$: which describes the convective cells
$\Theta_{2m,n}$: which describes the horizontal temperature difference in the convective cells
$\Theta_{2(0,2n)}$: which arises due to the distortion of basic temperature by convection.

With the intention of getting the classical Lorenz model in the limiting case, we scale the modes as given below,

$$\left.\begin{aligned}\Psi_{1\,m,n} &= \frac{\sqrt{2}\delta^2_{m,n}}{q\pi}X_{m,n},\ \Theta_{2m,n} = \frac{\sqrt{2}}{r\pi}Y_{m,n}\\ \Theta_{2(0,2n)} &= -\frac{\sqrt{2}}{\pi r}Z_n\end{aligned}\right\} \forall m,n, \quad (36)$$

where $r = \dfrac{Ra_{1,1}q^2\pi^2}{\delta^6_{1,1}}$, scaled modal Rayleigh number.

Published under an exclusive license by AIP Publishing

D. Minimal-modal fourier truncation

1. Third-order, autonomous system

The modes $m = 1$ and $n = 1$ represent the minimal Fourier truncation. By substituting minimal Fourier modes in the governing Eqs. (20)–(22) and multiplying the resultant equations, respectively, by the orthogonal eigenfunctions and integrating over one wavelength, we obtain

$$\frac{dX_{1,1}}{d\tau} = Pr[-X_{1,1} + rY_{1,1}(\xi_{1,1} - \zeta_{1,1}Z_1)], \tag{37}$$

$$\frac{dY_{1,1}}{d\tau} = X_{1,1} - Y_{1,1} - X_{1,1}Z_1, \tag{38}$$

$$\frac{dZ_1}{d\tau} = -b_1 Z_1 + X_{1,1}Y_{1,1}, \tag{39}$$

where

$$\tau = \delta_{1,1}t,\ \zeta_{1,1} = \frac{M_1(\pi^2 - \eta_{1,1}^2)}{\eta_{1,1}^2} \text{ and } b_1 = \frac{4\pi^2}{\delta_{1,1}^2}. \tag{40}$$

In general, $\zeta_{i,j}$, $i = j = 1, 2, 3, \ldots$ and b_l, $l = 1, 2, 3, \ldots$ are defined as

$$\zeta_{i,j} = \frac{M_1(\pi^2(2j-1)^2 - \eta_{i,j}^2)}{\eta_{i,j}^2} \text{ and } b_l = \frac{4l^2\pi^2}{\delta_{1,1}^2}. \tag{41}$$

2. Solution for the minimal mode at the steady state: Expression for the steady finite-amplitude Rayleigh number

The minimal Fourier truncated amplitude Eqs. (38) and (39) possess the following analytical solution:

$$\left.\begin{aligned} X_{1,1}^2 &= \frac{-W_1 + \sqrt{W_1^2 - 4W_2}}{2}, \\ Y_{1,1} &= \frac{b_1 X_{1,1}}{b_1 + X_{1,1}^2}, \quad Z_1 = \frac{X_{1,1}^2}{b_1 X_{1,1}^2} \end{aligned}\right\}, \tag{42}$$

where $W_1 = b_1[r(\xi_{1,1} + \zeta_{1,1}) - 2]$ and $W_2 = b_1^2(1 - r\xi_{1,1})$.

Equating the term $W_1^2 - 4W_3$ to zero, we get the following expression for the finite-amplitude Rayleigh number[26],

$$Ra_{1,1}^f = \frac{\delta_{1,1}^6}{\pi^2 q^2}\left(\frac{4\zeta_{1,1}}{(\xi_{1,1} + \zeta_{1,1})^2}\right), \tag{43}$$

where the superscript f indicates the finite-amplitude.

3. Analytical expression for the Hopf-Rayleigh number

The Rayleigh number at which the transition from regular convective motion to chaotic motion takes place is called the Hopf Rayleigh number, r_H. This is because at the Hopf Rayleigh number, the Hopf bifurcation of eigenvalue occurs. To find an analytical expression for r_H, the critical point (42) of the dynamical system (37)–(39) is considered.

Let us take

$$V(\tau) = V + \overline{V},$$

where $V = [X_{1,1}, Y_{1,1}, Z_1]^{Tr}$ and $\overline{V} = [\overline{X}_{1,1}, \overline{Y}_{1,1}, \overline{Z}_1]^{Tr}$ is one of the post-onset critical points of V, then the linearized system about the critical point, $\overline{V}$, is given by

$$\frac{dV}{d\tau} = LV, \tag{44}$$

where

$$L = \begin{bmatrix} -Pr & rPr(\xi_{1,1} - \zeta_{1,1}\overline{Z}_1) & -rPr\zeta_{1,1}\overline{Y}_{1,1} \\ (1 - \overline{Z}_1) & -1 & -\overline{X}_{1,1} \\ \overline{Y}_{1,1} & \overline{X}_{1,1} & -b_1 \end{bmatrix}. \tag{45}$$

The characteristic equation of Eq. (44) after substituting the critical points (42) is given by

$$f(\lambda) = -\lambda^3 + c_1\lambda^2 + c_2\lambda + c_3, \tag{46}$$

where

$$\begin{aligned} c_1 &= -(1 + b_1 + Pr), \\ c_2 &= -\frac{1}{(b_1 + s^2)^2}\left[b_1^3(1 + Pr) + s^4(Pr + s^2)\right. \\ &\quad + b_1^2(Pr + 3s^2 + Prs^2(2 - r\zeta_{1,1}) - rPr\xi_{1,1}) \\ &\quad \left. + b_1 s^2(3s^2 + Pr(2 + s^2 - r(\zeta_{1,1} - \xi_{1,1}))\right], \\ c_3 &= \frac{1}{(b_1 + s^2)^2}\left[Pr(-(b_1 + s^2)^3 - b_1 rs^2(-3b_1 + s^2)\zeta_{1,1}\right. \\ &\quad \left. + b_1 r(b_1^2 - s^4)\xi_{1,1}\right]. \end{aligned}$$

At $\lambda = i\lambda_1$, the eigenvalue, r, crosses the complex plane's imaginary axis, i.e.,

$$f(i\lambda_1) = \lambda_1^3 i - c_1\lambda_1^2 + c_2\lambda_1 i + c_3. \tag{47}$$

Equating real and imaginary parts of the above equation to zero and solving the resultant equations for r, we get the following expression for the Hopf–Rayleigh number:

$$r_H = l_1 - l_2\sqrt{l_3}, \tag{48}$$

where

$$\begin{aligned} l_1 &= \zeta_{1,1}^2\left(b_1^2 + 2(b_1 + 1)Pr + 2b_1 - 3Pr^2 + 1\right) \\ &\quad + 2\zeta_{1,1}\xi_{1,1}Pr\left(b_1^2 - 2b_1 Pr - 2b_1 - 3Pr^2 + 6Pr + 3\right) \\ &\quad - \xi_{1,1}^2 Pr^2\left(b_1^2 + 2b_1 Pr + 2b_1 + Pr^2 + 2Pr + 3\right), \\ l_2 &= -\zeta_{1,1}(b_1 - Pr + 1) + \xi Pr(b_1 + Pr - 1), \\ l_3 &= (1 + b_1 + 3Pr)^2\zeta_{1,1}^2 - 2Pr(5 - b_1^2 + 6Pr + 5Pr^2 \\ &\quad -4b_1(1 + Pr))\zeta_{1,1}\xi_{1,1} + Pr^2(3 + b_1 + Pr)^2\xi_{1,1}^2. \end{aligned}$$

It is to be noted that Eq. (48) is the expression of the Rayleigh number at which the Hopf bifurcation concerning onset of chaos occurs (as predicted by the minimal Fourier truncated model) and hence it

Published under an exclusive license by AIP Publishing

is referred to as the Hopf–Rayleigh number. At this value of r, the post-onset fixed point, $\overline{V}$, of the system (37)–(39) loses stability. In this case, a pair of complex conjugate eigenvalues of the linearized system around $\overline{V}$ crosses the complex plane's imaginary axis. At this juncture, it is important to recollect from Refs. 53, 68, and 69 that the regular convective regime's ultimate transition to the chaotic regime occurs via different routes. This aspect is discussed in more detail in Sec. III C on results and discussion.

E. Extended-ferromagnetic-Lorenz models

With the intention of studying the influence of higher-modal dynamics on the onset of ferroconvection and chaos, we consider the following modes:

(i) Horizontally extended mode,
(ii) Vertically extended mode and
(iii) Mixed mode.

Let us now derive the extended-ferromagnetic-Lorenz dynamical systems pertaining to aforementioned modes.

1. Higher-modal Fourier horizontal truncation: Five-dimensional system

We now increase the order of the horizontal mode by 1, i.e., $m = 2$ and $n = 1$. By substituting $m = 2$ and $n = 1$ in Eqs. (25)–(27) and plugging resultant equations into governing Eqs. (20)–(22), and multiplying by corresponding eigenfunctions and integrating over one wavelength, we obtain

$$\frac{dX_{1,1}}{d\tau} = Pr[-X_{1,1} + rY_{1,1}(\xi_{1,1} - \zeta_{1,1}Z_1)], \tag{49}$$

$$\frac{dX_{2,1}}{d\tau} = Pr\left[-\frac{1}{c_{2,1}}X_{2,1} + 9rc_{2,1}Y_{2,1}(\xi_{2,1} - \zeta_{2,1}Z_1)\right], \tag{50}$$

$$\frac{dY_{1,1}}{d\tau} = X_{1,1} - Y_{1,1} - X_{1,1}Z_1, \tag{51}$$

$$\frac{dY_{2,1}}{d\tau} = X_{2,1} - \frac{1}{c_{2,1}}Y_{2,1} - X_{2,1}Z_1, \tag{52}$$

$$\frac{dZ_1}{d\tau} = -b_1Z_1 + X_{1,1}Y_{1,1} + 2X_{2,1}Y_{2,1}, \tag{53}$$

where $c_{i,j} = \left(\frac{\delta_{1,1}}{\delta_{i,j}}\right)^2$, $i = j = 1, 2, \ldots$.

2. Higher-modal Fourier vertical truncation: Six-dimensional system

In the vertical truncation, we fix the value of m to be 1 and raise the value of n to 2. Now on substituting these values in Eqs. (25)–(27) and using the resulting approximate solution into governing Eqs. (20)–(22), and applying orthogonality conditions, we obtain

$$\frac{dX_{1,1}}{d\tau} = Pr\left[-X_{1,1} + rY_{1,1}(\xi_{1,1} - \zeta_{1,1}Z_1) + r\zeta_{1,2}Y_{1,2}(Z_1 - 2Z_2)\right], \tag{54}$$

$$\frac{dX_{1,2}}{d\tau} = Pr\left[-\frac{1}{c_{1,2}}X_{1,2} + r\xi_{1,2}c_{1,2}Y_{1,2} + r\zeta_{1,1}c_{1,2}(Z_1 - 2Z_2)Y_{1,1}\right], \tag{55}$$

$$\frac{dY_{1,1}}{d\tau} = X_{1,1}(1 - Z_1) - Y_{1,1} + X_{1,2}(Z_1 - 2Z_2), \tag{56}$$

$$\frac{dY_{1,2}}{d\tau} = X_{1,2} - \frac{1}{c_{1,2}}Y_{1,2} + X_{1,1}(Z_1 - 2Z_2), \tag{57}$$

$$\frac{dZ_1}{d\tau} = -b_1Z_1 + X_{1,1}(Y_{1,1} - Y_{1,2}), \tag{58}$$

$$\frac{dZ_2}{d\tau} = -b_2Z_2 + X_{1,2}Y_{1,1} + 2X_{1,1}Y_{1,2}. \tag{59}$$

3. Mixed-modal Fourier truncation: Ten-dimensional system

In the mixed mode Fourier truncation, we raise both horizontal and vertical modes by 1, i.e., we take $(m, n) = (2, 2)$ and thus, we consider double-Fourier series expansion for the stream function, temperature, and magnetic potential of Eqs. (25)–(27) with $(m, n) = (2, 2)$, substituting them in governing Eqs. (20)–(22) and using the orthogonality condition, we obtain

$$\frac{dX_{1,1}}{d\tau} = Pr\left[-X_{1,1} + rY_{1,1}(\xi_{1,1} - \zeta_{1,1}Z_1) + r\zeta_{1,2}Y_{1,2}(Z_1 - 2Z_2)\right], \tag{60}$$

$$\frac{dX_{1,2}}{d\tau} = Pr\left[-\frac{1}{c_{1,2}}X_{1,2} + r\zeta_{1,1}c_{1,2}(Z_1 - 2Z_2)Y_{1,1} + r\xi_{1,2}c_{1,2}Y_{1,2}\right], \tag{61}$$

$$\frac{dX_{2,1}}{d\tau} = Pr\left[-\frac{1}{c_{2,1}}X_{2,1} + 9rc_{2,1}(\xi_{2,1} - \zeta_{2,1}z_1)Y_{2,1} + 9r\zeta_{2,2}c_{2,1}Y_{2,2}(Z_1 - 2Z_2)\right], \tag{62}$$

$$\frac{dX_{2,2}}{d\tau} = Pr[-9X_{2,2} + r\xi_{2,2}Y_{2,2} - r\zeta_{2,1}(Z_1 - 2Z_2)Y_{2,1}], \tag{63}$$

$$\frac{dY_{1,1}}{d\tau} = -Y_{1,1} + X_{1,1}(1 - Z_1) + X_{1,2}(Z_1 - 2Z_2), \tag{64}$$

$$\frac{dY_{1,2}}{d\tau} = -\frac{1}{c_{1,2}}Y_{1,2} + X_{1,2} + X_{1,1}(Z_1 - 2Z_2), \tag{65}$$

$$\frac{dY_{2,1}}{d\tau} = -\frac{1}{c_{2,1}}Y_{2,1} + X_{2,1}(1 - Z_1) + X_{2,2}(Z_1 - 2Z_2), \tag{66}$$

Published under an exclusive license by AIP Publishing

$$\frac{dY_{2,2}}{d\tau} = -9Y_{2,2} + X_{2,2} + X_{2,1}(Z_1 - 2Z_2), \tag{67}$$

$$\frac{dZ_1}{d\tau} = -b_1 Z_1 + X_{1,1}(Y_{1,1} - Y_{1,2}) + Y_{2,1}(2X_{2,1} - X_{2,2}), \tag{68}$$

$$\frac{dZ_2}{d\tau} = -b_2 Z_2 + X_{1,2}Y_{1,1} + 2X_{1,1}Y_{1,2} + 2X_{2,2}Y_{2,1} + 3X_{2,1}Y_{2,2}. \tag{69}$$

F. Features of the extended-ferromagnetic-Lorenz models

The minimal and higher-modal systems of autonomous equations are invariant under the following transformation:

$$(X_{m,n},\ Y_{m,n},\ Z_n) \to (-X_{m,n},\ -Y_{m,n},\ Z_n) \text{ for } m > 0, n > 0. \tag{70}$$

Thus, all extended-ferromagnetic-Lorenz systems have this **symmetry**.

Further, we can easily prove that

$$\sum_{m=1}^{M}\sum_{n=1}^{N}\left[\frac{d}{dX_{m,n}}\left(\frac{dX_{m,n}}{d\tau}\right) + \frac{d}{dY_{m,n}}\left(\frac{dY_{m,n}}{d\tau}\right)\right] + \sum_{n=1}^{N}\frac{d}{dZ_n}\left(\frac{dZ_n}{d\tau}\right) = -\left(\sum_{m=1}^{M}\sum_{n=1}^{N}(Pr+1)\frac{1}{c_{m,n}} + \sum_{n=1}^{N} b_n\right) < 0. \tag{71}$$

Thus, extended-ferromagnetic-Lorenz systems are dissipative ones. We now prove that extended-ferromagnetic-Lorenz systems are energy-conserving in the limit of zero Prandtl number. To do so we consider the kinetic energy, T, and potential energies, U and V in a dimensionless form as shown below,

$$T = \frac{1}{2}\sum_{m=1}^{M}\sum_{n=1}^{N}\left[\left(\frac{\partial\psi_1(m,n)}{\partial z}\right)^2 + \left(-\frac{\partial\psi_1(m,n)}{\partial x}\right)^2\right], \tag{72}$$

$$U = -\frac{RaPr}{2}\sum_{m=1}^{M}\sum_{n=1}^{N}[\theta_2(m,n)^2 + \theta_2(0,2n)^2], \tag{73}$$

$$V = -\frac{RaPr}{2}\sum_{m=1}^{M}\sum_{n=1}^{N}[\phi_1(m,n)^2 + \phi_1(0,2n)^2]. \tag{74}$$

Substituting Eqs. (25)–(27) into Eqs. (72)–(74) and integrating over one fundamental wavelength, we obtain

$$\mathrm{T} = \frac{1}{2\pi^2}\sum_{m=1}^{M}\sum_{n=1}^{N}\delta_{m,n}^6 X_{m,n}^2, \tag{75}$$

$$\mathrm{U} = -\frac{RaPr}{2\pi^2 q}\sum_{m=1}^{M}\sum_{n=1}^{N}[Y_{m,n}^2 - Z_n^2], \tag{76}$$

$$\mathrm{V} = -\frac{RaPr}{2\pi^2 q}\sum_{m=1}^{M}\sum_{n=1}^{N}[\Phi_{1(m,n)}^2 - \Phi_{1(0,2n)}^2]. \tag{77}$$

To verify that the total energy, $\mathrm{E} = \mathrm{T} + \mathrm{U} + \mathrm{V}$, is conserved we consider

$$\sum_{m=1}^{M}\sum_{n=1}^{N}\frac{dE_{m,n}}{d\tau} = \frac{\delta_{1,1}^2}{\pi^2}\sum_{m=1}^{M}\sum_{n=1}^{N}\left\{\delta_{m,n}^6 X_{m,n}\frac{dX_{m,n}}{d\tau} - \frac{RaPr}{q}\left(Y_{m,n}\frac{dY_{m,n}}{d\tau} - Z_n\frac{dZ_n}{d\tau} + \Phi_{1(m,n)}\frac{d\Phi_{1(m,n)}}{d\tau} - \Phi_{1(0,2n)}\frac{d\Phi_{1(0,2n)}}{d\tau}\right)\right\}. \tag{78}$$

By substituting Eqs. (25)–(27), (32), and (36) in Eq. (78), we get

$$\sum_{m=1}^{M}\sum_{n=1}^{N}\frac{dE_{m,n}}{d\tau} = -\frac{\delta_{1,1}^2 Pr\ Ra}{\pi^2 q}\sum_{m=1}^{M}\sum_{n=1}^{N}\left\{\frac{\delta_{m,n}^2}{Ra}X_{m,n}^2, - \left(\frac{\eta_{m,n}^4 + \pi^2}{\eta_{m,n}^4}\right)Y_{m,n}^2 - \left(\frac{4\pi^2 n^2 + b_1}{4\pi^2 n^2}\right)Z_n^2 - \left[q^2\xi_{m,n} + \frac{\eta_{m,n}^4 + \pi^2}{\eta_{m,n}^4} - \left(\frac{4\pi^2 n^2 + b_1}{4\pi^2 n^2}\right)\right]Z_n X_{m,n} Y_{m,n}\right\}. \tag{79}$$

In the dissipationless limit, i.e., $Pr \to 0$, we have

$$\sum_{m=1}^{M}\sum_{n=1}^{N}\frac{dE_{m,n}}{d\tau} = 0, \tag{80}$$

which gives

$$\mathrm{E} = \sum_{m=1}^{M}\sum_{n=1}^{N}E_{m,n} = \text{ const.} \tag{81}$$

Hence, extended-ferromagnetic-Lorenz systems conserve energy in the dissipationless limit.

III. RESULTS AND DISCUSSION

This section is divided into four subsections and addresses the following aspects of the problem:

(i) Importance of the chosen problem,
(ii) Presentation of results from the linear theory and discussion on the same,
(iii) Extracting results from the nonlinear theory, especially in the chaotic regime and discussion on the same and
(iv) Studying the influence of non-dimensional parameters on the higher-order dynamics.

A. Importance of the chosen problem

Ferrofluid is a colloidal fluid synthetically prepared by suspending micrometer-sized ferromagnetic particles in a carrier fluid. Common choice of carrier fluid is electrically non-conducting fluids like water, synthetic oil, kerosene, and other such fluids. The suspended particles generally considered are made of ferrite, and hence heat transport in a ferrofluid is more significant than that in a carrier fluid without suspended particles. Thus, RBC in a ferrofluid termed as "thermomagnetic convection" or "ferroconvection," is a very useful mechanism in the situation when conventional convection fails to provide adequate heat. Study on ferroconvection as of

Published under an exclusive license by AIP Publishing

now has a history of 100 years and is still an ongoing and emerging research topic due to its numerous applications. Linear stability analysis of ferroconvection reported thus far by many researchers considers only the fundamental mode for predicting the onset of convection.[11,22,26,32,58] The same is the case with a nonlinear stability analysis of ferroconvection which uses one additional convective mode over the linear modes that facilitates the representation of nonlinearity in the resulting dynamical system. Such a minimal system, proposed by Saltzman[60] and used extensively by Lorenz[42] makes a choice favoring the nonlinearity in the equation of conservation of energy rather than the one in the equation of conservation of linear momentum. As is now well known,[22,26,42] the assumption of small-scale convective motions allows one to make such a choice of a minimal system. The latter system proved to be an acceptable one since many gross features of the original system were predicted by the minimal modes and is thus to this day a truly amazing result. In course of time, the natural question that arose in the mind of researchers is whether the minimal system misses some of the features of the original system both quantitatively and qualitatively. The noteworthy works in this direction are those of Lorenz,[70] Roy and Musielak,[61] Musielak *et al.*,[64] Shen,[65] and Siddheshwar.[71] The research team of Musielak[61–64] provided answers to such questions in the case of Newtonian fluids. The experimental result by Gollub and Benson[72] and numerical simulation by Curry *et al.*[73] and Yahata[74,75] delineate results connected with the routes to chaos via quasiperiodicity and phase-locking in higher-order Lorenz systems. The importance of knowing which particular mode yields the least eigenvalue and whether it is the fundamental mode that yields such a value (as in the case of a Newtonian fluid) makes the corresponding problem in a Newtonian ferromagnetic fluid an interesting one. Further, another question that arises is: does the minimal mode continue its domination over other modes in the convective regime to the point of the onset of chaos and beyond is a matter of greater interest.

It is well known that the tri-modal Lorenz model with two nonlinearities is the optimal one for studying onset of convection in a Newtonian fluid, whereas in the case of the Newtonian ferrofluid, it is the tri-modal magnetic-Lorenz model that has three nonlinearities. In the literature, the former Lorenz model is known as the classical Lorenz model and the latter one is known as the Glukhovsky–Dolzhansky system or the magnetic-Lorenz system. This system is also observed in the problems of convective fluid motion within an ellipsoidal rotating cavity (see Glukhovskii,[76] Garashchuk *et al.*[77]), electroconvection (see Siddheshwar and Radhakrishna[71]) and in other applications (see Kuznetsov *et al.*,[78] Leonov *et al.*[79]). In view of the observations made so far the onset of regular/chaotic ferroconvection is studied in the paper using fundamental and higher modes as proposed by Saltzman,[60] and their effects are delineated. Effect of magnetic particles and different modes on known characteristics of the classical Lorenz and the classical magnetic-Lorenz systems are studied elaborately. Preference of modes during onset of regular motion and chaotic ferroconvective motion is analyzed. The plots of the largest Lyapunov exponent (LLE) and the bifurcation diagram are used in predicting different convective regimes [regular, mildly-chaotic (periodic) with different periods] and in specifically studying chaotic behavior of the dynamical system. In order to show the existence of hyper chaos in the higher-order dynamical system, we have calculated the second largest Lyapunov exponent (SLLE) besides the calculation of LLE values. These values were computed using the algorithm proposed by Wolf *et al.*[80] In the literature, this method has also been used by many in their study of other dynamical systems.[69,81–88]

The discussion of the results focuses on the following two aspects:

(i) Onset of regular cellular-convection—infinitesimal/finite-amplitude convection and
(ii) Onset of chaos and its sustenance or otherwise.

The following truncated-Fourier series solutions are considered to arrive at four different dynamical systems of various orders:

(a) Minimal modes by taking horizontal and vertical modes as $m = 1$ and $n = 1$ respectively,
(b) Horizontally extended mode by taking horizontal and vertical modes as $m = 2$ and $n = 1$, respectively,
(c) Vertically extended mode by taking horizontal and vertical modes as $m = 1$ and $n = 2$, respectively and
(d) Mixed mode by taking horizontal and vertical modes as $m = 2$ and $n = 2$, respectively.

We need to mention here that in addition to these modes those pertaining to the convective regime are considered.

B. Onset of regular cellular convection: Possibility of subcritical motions

Before writing about the linear stability analysis, we note that for a fixed value of the aspect ratio, h/l, we consider integer multiples (m) of it in the x-direction as periodicity is observed in the appearance of longitudinal rolls considered in the paper. Integer multiples of the aspect ratio also signify that the solution takes care of the vertical wall effect. The integer m indicates the number of cells in the box that depends on the aspect ratio and that it can either be even or odd. In the case of an even value, it indicates that there are as many counter-rotating cells as there are clockwise rotating ones, while in the case of an odd value, there will be one more of either of the two cells. In the z-direction, the solution is chosen in such a way that the real part or the imaginary part of the variable-separable solution satisfies the boundary condition. Integer multiples (n) of the argument of the exponential function of z also satisfy the boundary conditions. In any case, the choice of the exponential function instead of the trigonometric functions is due to the ease of calculations.[67]

With the intention of validating the results of the problem undertaken, we reproduced some of the results of previous investigations which includes

(a) Obtaining the results of the classical problem RBC as a limiting case by taking $M_1 = 0$ and
(b) proving the possibility of subcritical motion in the present problem.

Figure 2 is a plot of the Rayleigh number vs the wave number plotted using the solution of the minimal-mode truncated-Fourier series for two different values of M_1, i.e., $M_1 = 0$ and $M_1 = 2$. Here, $M_1 = 0$ corresponds to the case of no magnetic field or the classical problem

Published under an exclusive license by AIP Publishing

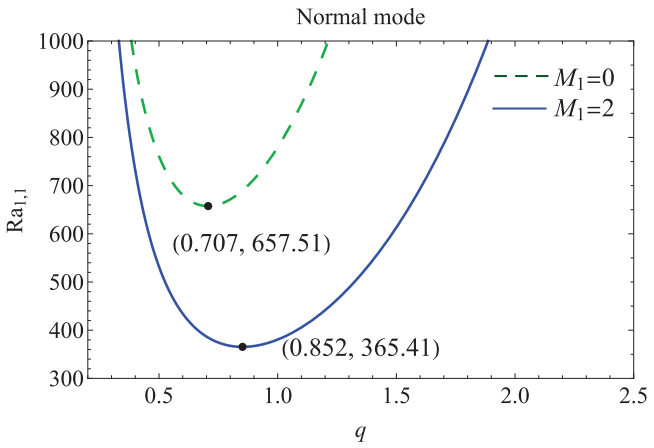


FIG. 2. Plot of Rayleigh number vs wave number for different values of M_1 and for $M_3 = 1.1$.

of RBC. It is evident from Fig. 2, that in the case of no magnetic field, we get the results of the classical RBC and this validates the double Fourier series solution that we have taken. It is also evident from Fig. 2 that the influence of the imposed external magnetic field is to advance the onset of ferroconvection. For $M_1 = 2$ and $M_3 = 1.1$, we see here that the percentage of reduction of value of the critical Rayleigh number is of 45% to reach 55% of its initial value.

In order to prove that sub-critical motions are possible, we derived the steady state solution of the minimal modal dynamical system (37)–(39) and obtained the finite-amplitude Rayleigh number (43). Using Eqs. (34) and (43), we can write

$$\frac{Ra^f_{1,1}}{Ra_{1,1}} = \frac{4\zeta_{1,1}}{\xi_{1,1}(\xi_{1,1}+\zeta_{1,1})^2}. \tag{82}$$

For the given value of parameters, i.e., $M_1 = 2$ and $M_3 = 1.1$, we get

$$\frac{Ra^f_{1,1}}{Ra_{1,1}} < 1. \tag{83}$$

Thus, we see that sub-critical motions are possible in the problem. Figure 3 reproduces similar results. Furthermore, Fig. 3 confirms that, in the absence of the magnetic field, the sub-critical motion is not possible. Influence of higher modes is discussed using Fig. 4 and Table I.

Plots in Fig. 4, respectively, represent the variation of Ra with wave number obtained using the Fourier series solution of the minimal mode ($Ra_{1,1}$) and those of the higher horizontal mode ($Ra_{2,1}$), the higher vertical mode ($Ra_{1,2}$) and mixed mode ($Ra_{2,2}$). From these plots, we may conclude the following:

$$Ra_{1,1} = Ra_{2,1} \ll Ra_{2,2} = Ra_{1,2}. \tag{84}$$

This implies that the preferred mode for the ferroconvection problem is the minimal mode and horizontally extended-Fourier mode. In Sec. III C, we study the effect of higher modes on the onset of chaotic motion in the system using the largest Lyapunov exponent(LLE), the bifurcation diagram, and the phase-space plots.

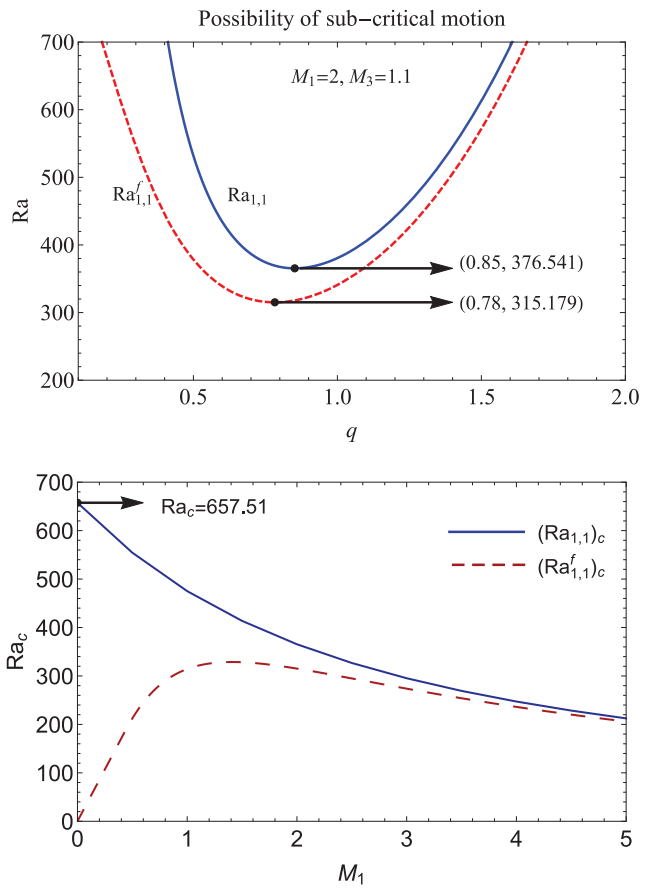


FIG. 3. Plot of the Rayleigh number of linear and weakly nonlinear theories (using normal modes) vs the wave number (left) and vs M_1 (right) for $Pr = 10$.

C. Onset of chaotic motion

An analytical expression for the Hopf Rayleigh number, r_H, using the minimal mode at which the equilibrium or critical points lose stability through a Hopf bifurcation is explicitly reported in the paper [see Eq. (48)]. Using this expression, r_H is plotted vs M_1 and shown in Fig. 5.

It is clear from Fig. 5 that the transition from regular convective motion to chaotic motion takes place at $r_H = 6.5$ for $M_1 = 2$, $M_3 = 1.1$ and $Pr = 10$ for the case of the minimal mode. As M_1

TABLE I. Table for critical Rayleigh number and wave number for different modes by taking $M_1 = 2$ and $M_3 = 1.1$.

Modes	(m, n)	Ra_c	q_c
Minimal mode	(1,1)	365.408	0.852
Horizontally extended mode	(2,1)	365.408	0.284
Vertically extended mode	(1,2)	29 598	2.555
Mixed mode	(2,2)	29 598	0.852

Published under an exclusive license by AIP Publishing

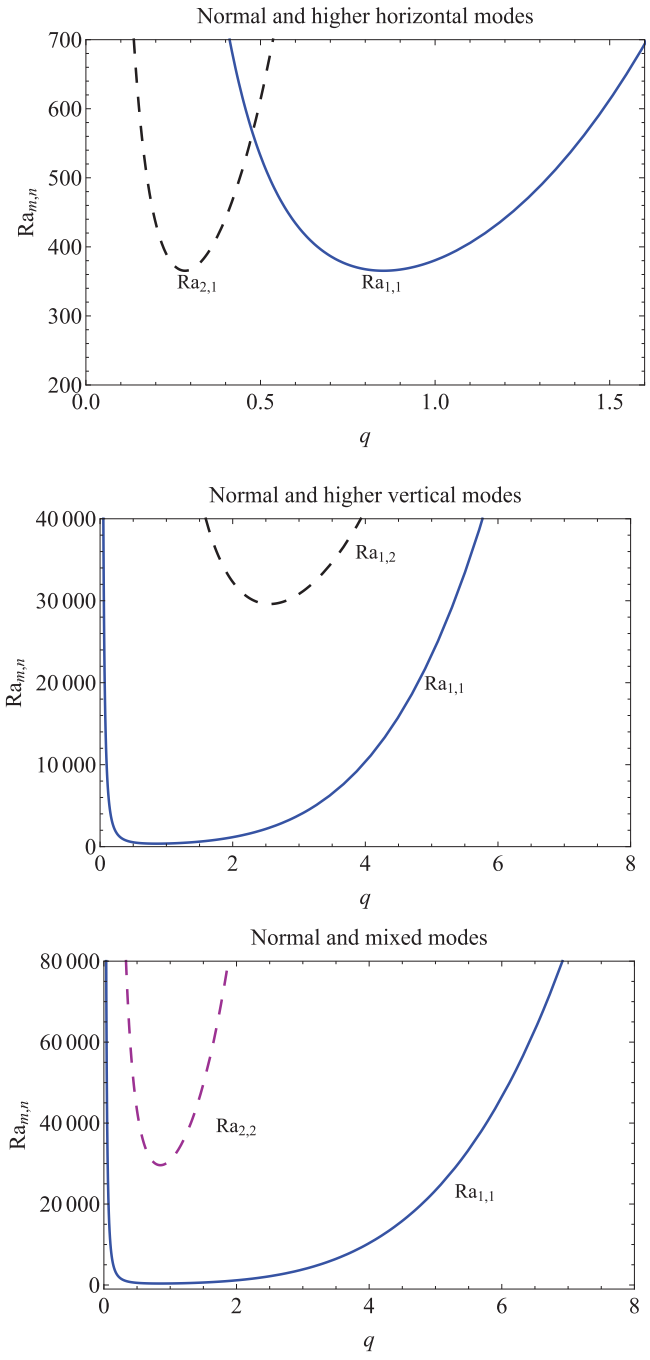


FIG. 4. Plots of the modal Rayleigh number vs wave number for different modes by taking $M_1 = 2$ and $M_3 = 1.1$.

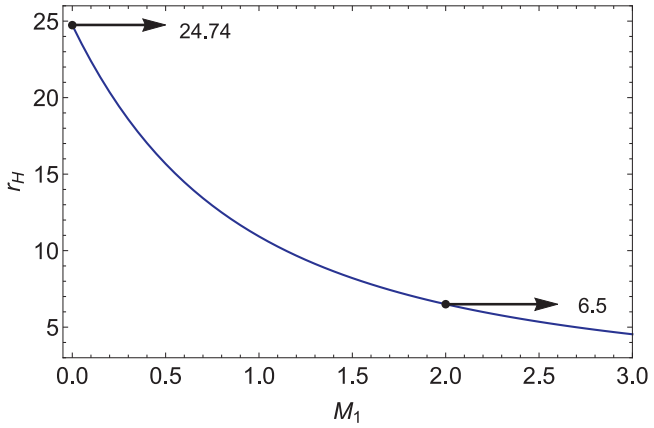


FIG. 5. The Hopf–Rayleigh number vs M_1 obtained using the minimal-mode truncated Fourier solution for $M_3 = 1.1$, $Pr = 10$, and $q = 0.854$.

increases, the value of r_H decreases. Thus, in the case of the minimal-mode system, increase in the value of M_1 is to advance the onset of chaos. In the limiting case of M_1=0 (classical RBC), we obtained $r_H = 24.74$ which was the value obtained by Lorenz[42] and reported by others also.[69,89] Thus, this result of the present study stands validated in comparison with the results of previous investigators in the limiting case of the classical Lorenz model.

To study the dynamical behavior of the systems obtained from minimal and higher-modal Representations, we have computed the Lyapunov spectrum, the bifurcation diagram, and the phase-space plots. The numerical integration of the equation is done using the standard fourth-order Runge–Kutta method with a time step of $\Delta\tau = 10^{-5}$. We have used this small discretization to ensure the convergence of the dynamical states in all reduced models. In particular, the ten-dimensional model requires this $\Delta\tau$.

The Lyapunov spectrum was computed using the algorithm proposed by Wolf *et al.*[80] The elements of the Lyapunov spectrum are arranged in the descending order: $\lambda_1 \geqslant \lambda_2 \geqslant \lambda_3 \cdots \geqslant \lambda_N$, where N is equal to the order of the dynamical system's dimension. The first one is known as the largest Lyapunov exponent (LLE) and the second one is the second largest Lyapunov exponent (SLLE). Let us remark that if $LLE < 0$, the system is in a fixed-point state, if the $LLE = 0$ and $SLLE < 0$, the system is in a periodic-state, if $LLE = 0$ and $SLLE = 0$, the system is in a quasi-periodic state, if the $LLE > 0$ and $SLLE \leqslant 0$, the system is in a chaotic state, whereas if $LLE > 0$ and $SLLE > 0$, the system is in a hyper-chaotic state.[85] The bifurcation diagram is obtained by recording the local maximum of one of the amplitudes extracted from its time series plot. To explore main differences among modal expansions, we vary r and fix the remaining parameters at $M_1 = 2$, $M_3 = 1.1$, and $Pr = 10$. In particular cases, we report the influence of non-dimensional parameters by considering random values for M_1, M_3, and Pr. Further, the initial conditions also are considered randomly. In order to ensure convergence and to minimize the numerical error, the maximum time for plotting the LLE and bifurcation diagrams for minimal, horizontally extended and vertically extended modes is taken to be 2×10^5 time steps after the transient, whereas for the mixed mode, it is taken to be 1×10^6 time steps after the transient. To decide on these values, many trial runs were made.

Published under an exclusive license by AIP Publishing

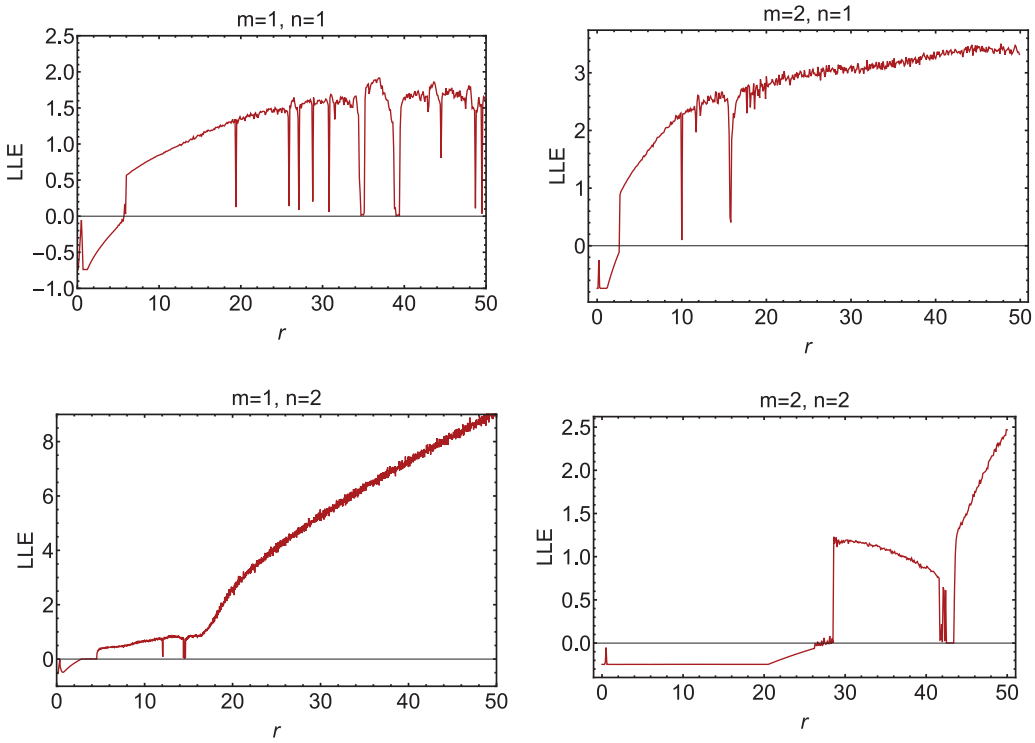


FIG. 6. Plots of the largest Lyapunov exponent(LLE) vs scaled Rayleigh number(r) using the minimal and higher-order Fourier series expansions for $M_1 = 2$, $M_3 = 1.1$, $Pr = 10$, and $\tau^{Max} = 1000$.

In order to characterize the results concerning regular and chaotic convection, we first compute LLE as a function of r and this is shown in Fig. 6. First, let us consider that portion of the LLE plots in which the exponent is negative. In this regime of convection, we notice a sudden spurt in the value of r that gets closer to 0 but stops short of it. It must be noted here that the peak of such a spurt is, in fact, the value r_c at which the primary instability of regular cellular motion commences. The end of the regime of regular convection is signified by the LLE ceasing to be negative. This zero value of the LLE signifies the threshold of the regime of chaotic motion. Beyond this value, r_{ch}, at which the LLE becomes 0 we must keep in mind the fact that the LLE thereon does not become negative though it might closely get near 0 for some values of r. For most part of the chaotic regime, the LLE displays an oscillatory behavior and such behaviors are interspersed with regimes in which the chaos seems to fizzle out by losing energy only to gain energy again and display chaos. In the many sapped-energy regimes, the LLE assumes very small values close to zero and then the system is forced to perform periodic motions of various periods.

One can observe from the plots of the LLE in Fig. 6 that there are interruptions in the chaotic motion as r increases beyond r_{ch} and at such values of r, the system experiences a peculiar situation wherein the system has neither chaos nor periodic motion and such nearly-periodic regimes are also referred to as mildly chaotic ones. The list of such mildly chaotic points/interval for all the modes are documented in Table II. From Table II, it is clear that compared to the higher modes (all three types) there are many such dips (nearly/fully periodic points) in the case of the minimal mode. As the

TABLE II. Values of Rayleigh numbers when the chaotic state commences, r_{ch}, and for the subsequent periodic windows for minimal and higher-mode solutions at $M_1 = 2$, $M_3 = 1.1$, $Pr = 10$, and $\tau^{Max} = 1000$.

Modes	(m, n)	r_{ch}	Nearly periodic points	Fully periodic points
Minimal mode	(1,1)	6.5	19.4, 27.1	25.9, 28.8, 30.8, 35
Horizontally extended mode	(2,1)	2.8	10, 12.25	15.8
Vertically extended mode	(1,2)	4.5	12.05	[2.8,4.4], 14.4
Mixed mode	(2,2)	28.6	…	[41.7,42.1], 42.3,[42.5,43.3]

Published under an exclusive license by AIP Publishing

number of modes increases, appearance of such dips decreases indicating a vigorous-chaotic system. This compels us to think that the existence of nearly periodic motion is a consequence of truncation and that it disappears on adding modes.

In the case of horizontally and vertically extended modes, from the corresponding plots in Fig. 6 we notice that in the r-interval [30,50], there are no dips for plots of the LLE and hence we considered the interval [0,30] in the plots for the LLE in Fig. 6. However, for a given range of r, in the case of vertical and mixed modes, we noticed that after the transition from the regular convective motion to the chaotic motion, the system attains a vigorous-chaotic-state with two-time interruptions of chaotic motion by periodic motion. In the case of horizontal mode extension, however, the dynamical system shows suppression of intensity of chaos as r increases. Thus, we infer from our findings that as the vertical mode is increased, the dynamical system displays delayed onset of chaos but exhibits vigorous chaos compared to that by the horizontal mode.

For the purpose of comparing the state-difference among the considered modes, we have defined a binary indicator, Δ, based on the LLE that measures the difference of states. For two states "a_1" and "a_2," the indicator is defined as follows:

$$\Delta = \begin{cases} 0, & \text{if } sign(LLE, a_1) = sign(LLE, a_2), \\ 1, & otherwise. \end{cases} \tag{85}$$

Figure 7 is a plot of the state difference indicator between the minimal and higher-order modes as a function of r plotted using Eq. (85).

In the state-difference plots in Fig. 7 when there is a match of the type of states then the color code of green is used whereas yellow is used otherwise. These state-difference plots in Fig. 7 disclose that the dynamical behavior of the vertical and the horizontal modes are inherited from that of the minimal mode with only shift in the value of r where periodic motion occurs. Thus, the difference between these states is almost similar. Further, it is noticed that the difference in states is significantly great in the case of the comparison between the minimal and mixed-mode ($\Delta_{2,2}$), compared to that between the minimal and horizontal modes ($\Delta_{2,1}$) and the minimal and vertical mode ($\Delta_{1,2}$). The strong discrepancy between the values of the LLE predicted by the minimal and the higher-order systems can be explained as follows. It appears from Fig. 7 that some neglected higher-modes in the lower-order model carry more energy than the lower modes alone and hence we see the discrepancy in the state difference indicator of lower and higher-order models. This could mean that as r increases the higher mode take over from the lower mode. Further our study about the dynamical behavior of the system associated with the mixed-mode one (higher-order) is provided in Sec. III D.

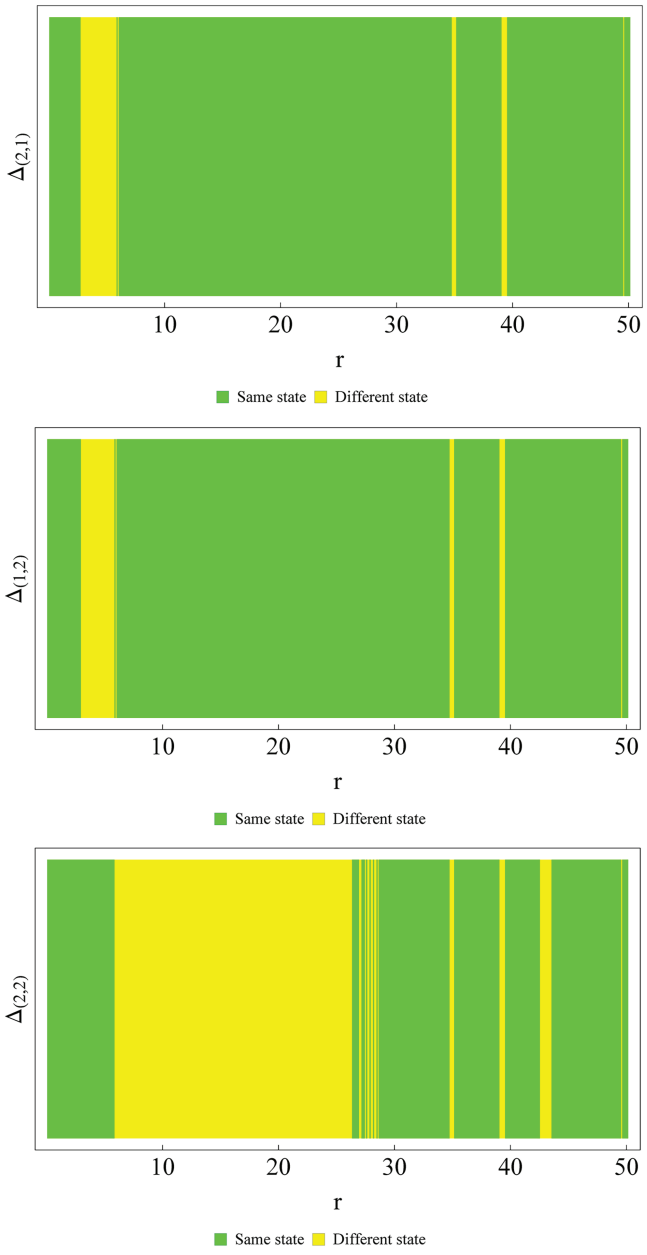


FIG. 7. Plot of the state difference indicator, Δ, between the minimal and higher-order systems as a function of r.

D. Dynamical behavior of the tenth-order dynamical system associated with the mixed-mode

This subsection is solely dedicated to understanding the influence of the non-dimensional parameters on the dynamics described by the tenth-order dynamical system obtained using the mixed-mode Fourier series expansion (the highest-order considered in the paper). At this stage, we note from the LLE plot concerning the mixed-mode Fourier expansion in Fig. 6 that chaos commences for this higher-order system at $r = 28.6$ for fixed values of Pr, M_1, and M_3. In this section, we consider moderate values of the non-dimensional parameters and study their influence on the dynamics.

First and foremost, we study the influence of the Prandtl number on the tenth-order dynamics. Figure 8 is the plot of LLE vs the Prandtl number (Pr) for the tenth-order system by taking $r = 40$ and

Published under an exclusive license by AIP Publishing

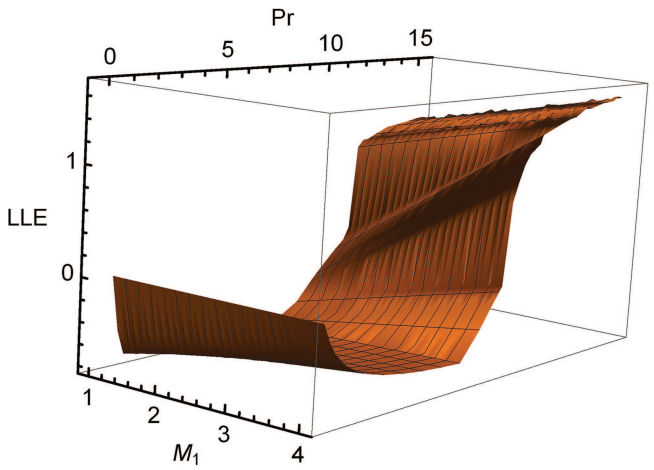


FIG. 8. Plot of the LLE vs Prandtl number for the mixed truncated Fourier series expansion system, for different values of M_1 and for $M_3 = 1.1$ and $r = 40$.

TABLE III. Values of Prandtl number (Pr) in different regimes of the mixed truncated Fourier series expansion system, for different values of M_1 and for $M_3 = 1.1$ and $r = 40$.

	Values of Pr	
M_1	Regular convective regime (LLE < 0)	Chaotic regime (LLE > 0)
1	[0,10.81]	[10.82,15]
2	[0, 9.53]	[9.54, 15]
3	[0, 8.65]	[8.66, 15]

$M_3 = 1.1$, and plotted for different values of M_1. The small values of Pr indicate the situation wherein the heat diffuses quickly compared to the diffusion of linear momentum. The declined values of LLE in the regular convective regime ($LLE > 0$) indicate this situation. In Table III the values of Pr for various regimes are documented. It is clear from this table that as we increase M_1, the chaos sets-in for a

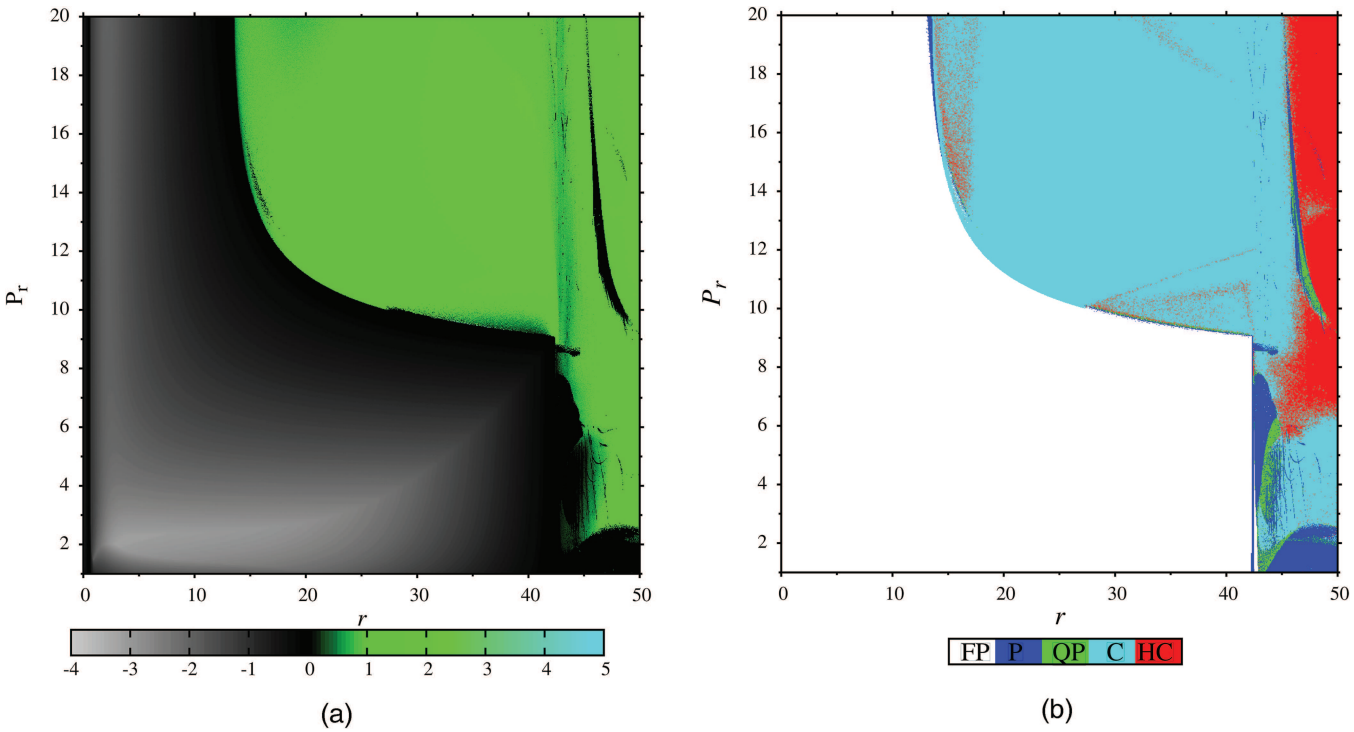


FIG. 9. Color-coded phase diagrams of the LLE (a) and the dynamical states (b) as a function of r and Pr for the mixed truncated Fourier series expansion system at $M_1 = 2$ and $M_3 = 1.1$. In panel (b), the fixed point, periodic, chaotic, and hyper-chaotic states are denoted by FP, P, QP, C, and HC, respectively. Also, these states are represented by white, blue, green, cyan, and red colors, respectively. (a) Phase diagram of LLE. (b) Phase diagram of the dynamical states taking account of both LLE and SLLE to distinguish the states.

Published under an exclusive license by AIP Publishing

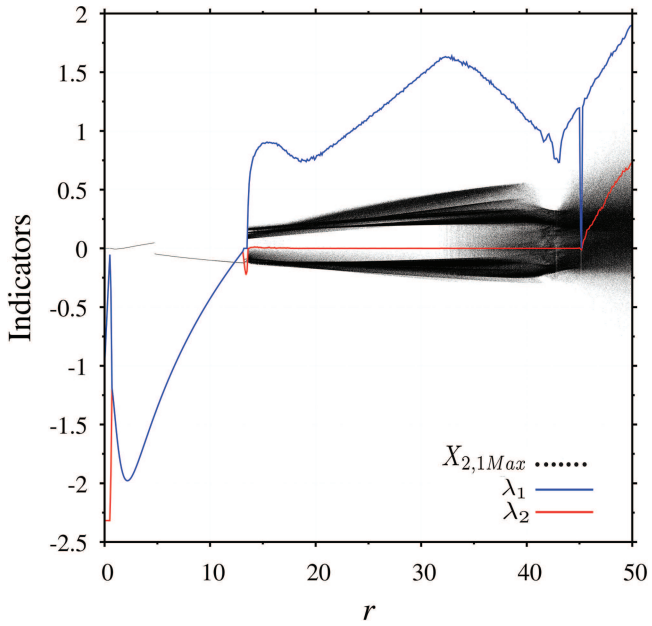


FIG. 10. The largest Lyapunov exponent(λ_1), the second largest Lyapunov exponent (λ_2), and the local maximum of amplitude, $X_{2,1}$, as a function of r for the mixed truncated Fourier series expansion system, for $Pr = 20$, $M_1 = 2$, $M_3 = 1.1$.

low Pr. Thus, the influence of M_1 is to enhance momentum diffusion of the system and thereby to advance the onset of chaos.

The plot of the LLE as a function of Pr and r is presented in Fig. 9. The black and green colored regimes in Fig. 9(a), respectively, represent the value of the LLE less than and greater than zero. With this information, it is pretty clear that the black color regime in Fig. 9(a) denotes the regular convective regime, while the green one represents the chaotic regime. From this plot, one can see that, when Pr is very small, the fixed point attractor switches directly to the periodic state via a quasi-periodic state. This indicates that the present dynamical system remains in the periodic state with less vigorous-chaotic convection or even no chaos in the case of very small Pr. Further, it is evident from Fig. 9 that one can find a threshold value of Pr upto which the value of r_{ch} at which the onset of chaos happens remains unchanged and after this threshold value, say, $Pr = 9.5$, the change of state from regular convective motion to chaotic motion depicted by r_{ch} is characterized by a decreasing function of r. In other words, the onset of chaos is advanced when $Pr > 9.5$. This leads us to the conclusion that, at values of Pr greater than the threshold value, in which the viscosity dominates over the thermal conductivity of the fluid, advanced onset of chaotic motion is seen. Thus, for high-viscosity fluids, one can expect onset of chaotic motion for small values of r.

The unstable behavior of the system in the post-chaotic-onset regime is depicted in Fig. 9(b). The system in the post-chaotic-onset regime undergoes several transitions among dynamical states, for example, a periodic (P), a quasi-periodic (QP) a chaotic (C) or also

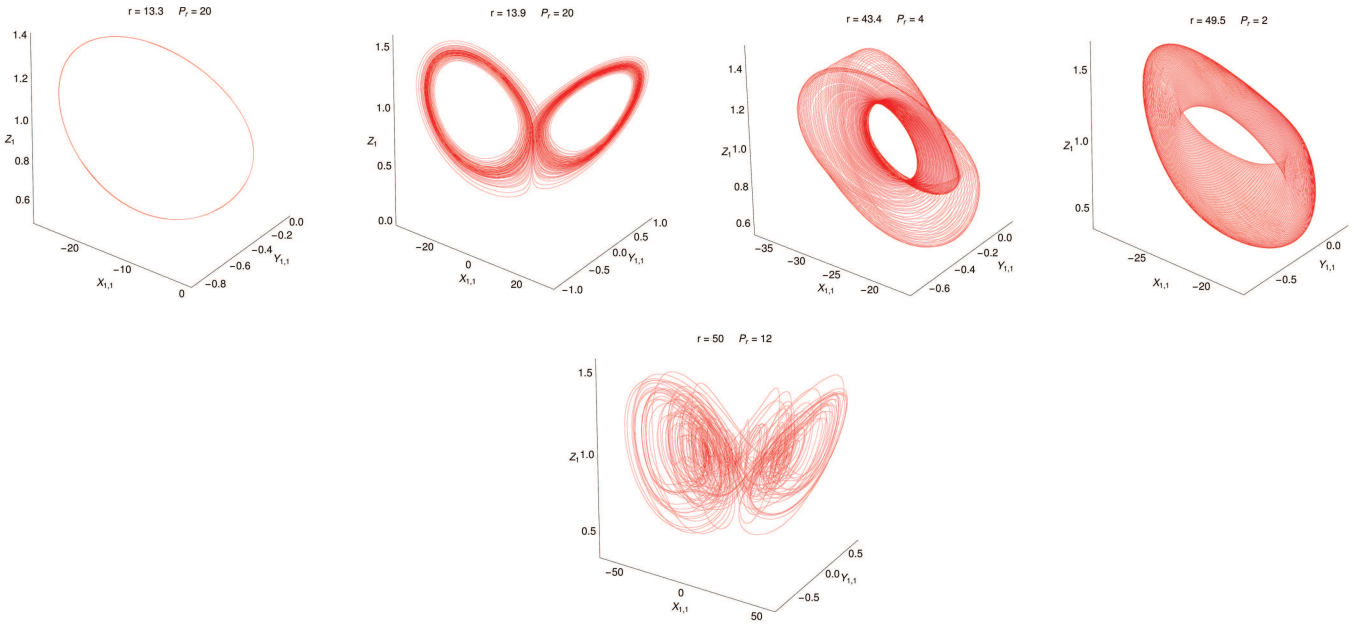


FIG. 11. The phase-space plots for various states plotted for the mixed truncated Fourier series expansion system by taking $M_1 = 2$ and $M_3 = 1.1$.

Published under an exclusive license by AIP Publishing

TABLE IV. Various states of the system for different values of r and Pr tabulated using information from Fig. 11.

r	13.3	13.9	43.4	49.5	50
Pr	20	20	4	2	12
Attractor	Limit cycle	Chaotic	Quasi-periodic	Quasi-periodic	Hyper-chaotic

an hyper-chaotic (HC) state. These seemingly complex transitions of the system at moderated values of r are captured in Fig. 9(b) using the LLE and SLLE values computed for different values of r and Pr, and for fixed values of $M_1 = 2$ and $M_3 = 1.1$. From this plot, we found that for values of Pr less than the threshold value, i.e., $Pr < 9.5$, and very much greater than the threshold value, i.e., $Pr \gg 9.5$, the break down of the regular convective motion to the chaotic motion does not occur abruptly. The system remains in the energy-conserving mode in a small interval of r and once it gets adequate energy then it shows up chaotic motion/oscillation. This also implies that in these cases, i.e., $Pr < 9.5$ and $Pr \gg 9.5$, r_{ch} at which the transition from the fixed point to the chaotic state occurs is not through a Hopf bifurcation. However, when Pr is slightly greater than its threshold value, say $Pr > 10$, then the scenario is opposite. In that case, the breakdown of the regular convective motion to chaotic motion occurs immediately and thus resembles the case of the minimal model reported by Lorenz,[42] where the transition to chaos is always through a Hopf bifurcation and the scaled Rayleigh number, r_{ch}, is r_H, a Hopf Rayleigh number. The LLE value around r_{ch} in Fig. 6 also reiterates the same situation. Thus, the influence of Pr is crucial so far as chaotic motion is concerned.

Transition from the periodic to a chaotic state sometimes occurs through the quasi-periodic state as shown in Fig. 9. An interesting fact from the tenth-order system is the existence of a hyper-chaotic behavior for large values of r. In this hyper-chaotic regime, the largest Lyapunov exponent and the second largest Lyapunov exponent, say λ_1 and λ_2, are positive as shown in Fig. 10. The bifurcation for the same is also provided in the figure as an evidence to this fact.

Figure 9(b) shows that this transition from chaotic to hyper-chaotic state is mediated by unstable periodic orbits. In fact, these unstable periodic orbits become repellers in the neighborhood of

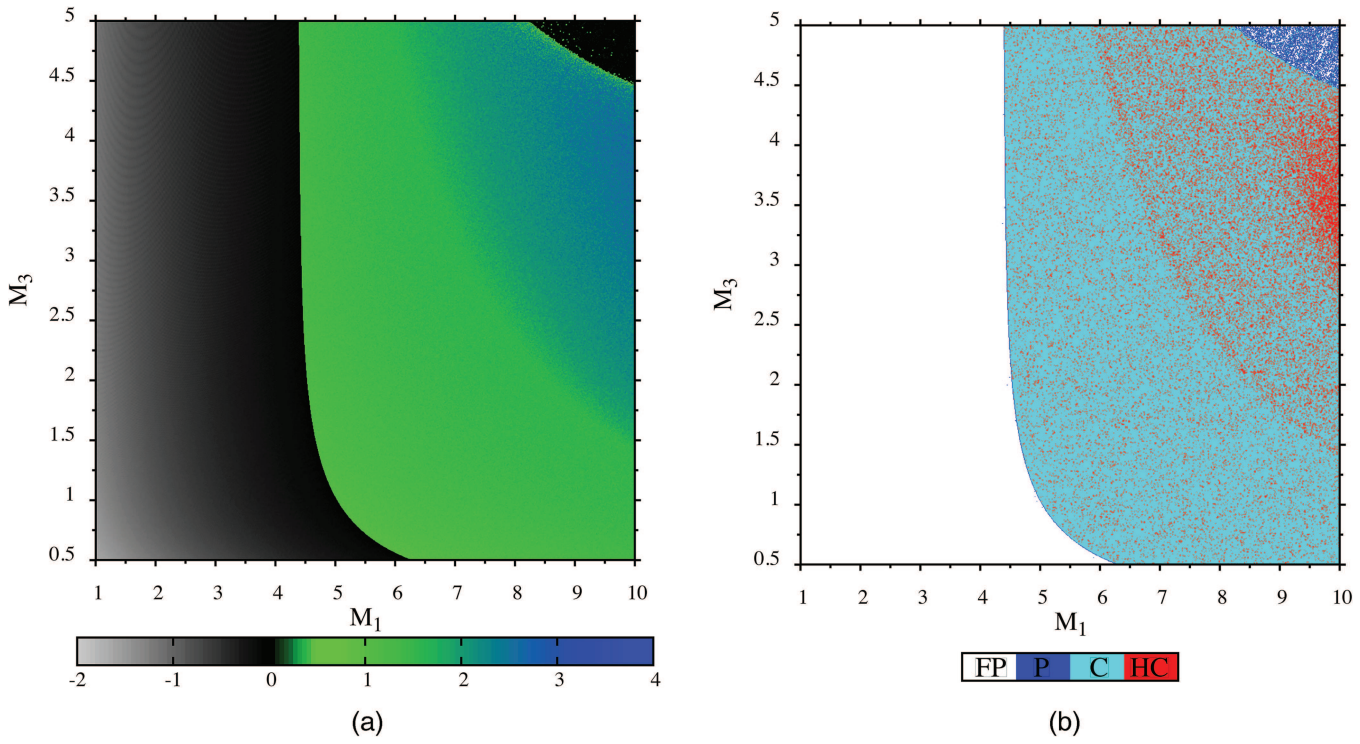


FIG. 12. Color-coded phase diagrams of the LLE (a) and the dynamical states (b) as a function of M_1 and M_3 for the mixed truncated Fourier series expansion system at $r = 10$ and $Pr = 10$. In panel (b), the fixed point, periodic, chaotic, and hyper-chaotic states are denoted by FP, P, C, and HC, respectively. Also, these states are represented by white, blue, cyan, and red colors, respectively. (a) Phase diagram of the LLE. (b) Phase diagram of the dynamical state taking account both of LLE and SLLE to distinguish the states.

Published under an exclusive license by AIP Publishing

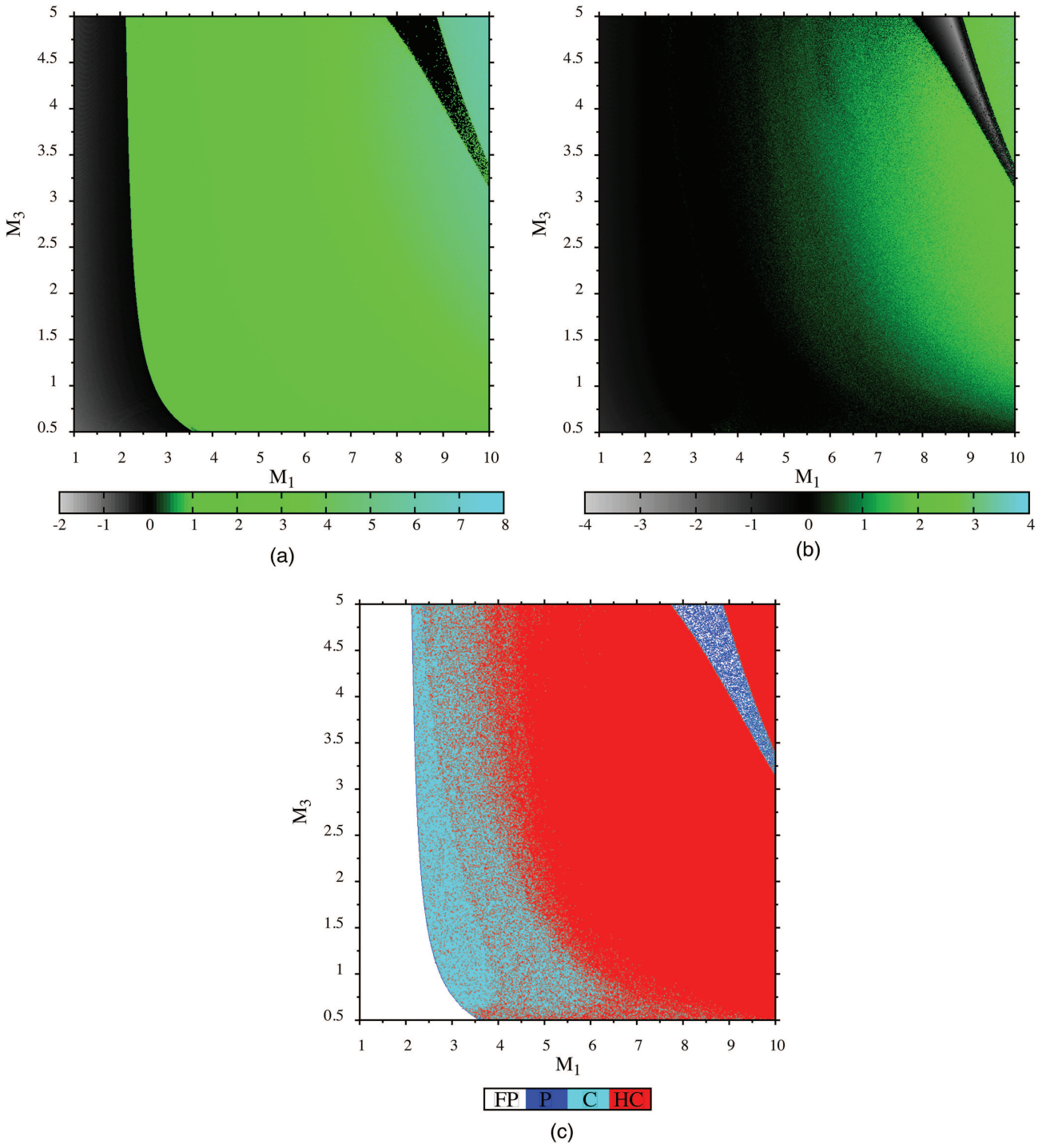


FIG. 13. Color-coded phase diagrams of the LLE (a), SLLE (b) and the dynamical states (c) as a function of M_1 and M_3 for the mixed truncated Fourier series expansion system at $r = 20$ and $Pr = 10$. In panel (c), the fixed point, periodic, chaotic, and hyper-chaotic states are denoted by FP, P, C, and HC, respectively. Also, these states are represented by white, blue, cyan, and red colors, respectively. (a) Phase diagram of the LLE. (b) Phase diagram of the SLLE. (c) Phase diagram of the dynamical state taking account both of LLE and SLLE to distinguish the states.

Published under an exclusive license by AIP Publishing

this transition. The phase-space plots for various states, i.e., fixed point(FP), chaotic(C), periodic(P), quasi-periodic(QP), and hyper-chaotic(HC) states, are presented in Fig. 11 for various values of r and Pr. These values of r and Pr and the information on the corresponding attractors are summarized in Table IV. Influence of magnetization parameters, M_1, and M_3, on the post-chaotic-onset regime is studied using Figs. 12 and 13. The phase diagram of the LLE as a function of M_1 and M_3, for the mixed-mode system depicted in Figs. 12 and 13 are plotted respectively for $r = 10$ and $r = 20$. It is clear from Fig. 12 that the influence of increase in the value of M_3 is to advance the onset of chaos. An appropriate range for M_3 can be detected from this figure where its influence is significant on r_{ch}. Since this plot is for $r = 10$, the appearance of the periodic or hyper-chaotic regime is sparse.

On seeing Fig. 13 in conjunction with Fig. 12, we note that when $r = 10$, in the post-chaotic-onset regime, the chaotic state is the most common state while when $r = 20$ the hyper-chaotic state is the dominant state of the system. Further, the possibility of the appearance of the periodic or the quasi-periodic state is less. This provides vital clue to us that the influence of the presence of the magnetic effect is to maintain the system in chaotic or even hyper-chaotic state without fizzling out to the periodic or quasi-periodic state.

One of the important applications of the chaotic/hyper-chaotic dynamics is the secure communication system which is most essential to any country. Encryption/decryption of the information arising from chaotic/hyper-chaotic signals facilitates the synchronization of the properties of the Lorenz system with an analog circuit which can be used for secure communication.[90,91] There is a distinct possibility that higher-order Lorenz models can be used in place of lower-order ones to ensure superior and secure communication.

IV. CONCLUSION

Usage of ferrofluid in heat transfer applications is an industry trend due to many reasons. The main reason for this is the particles' attraction toward the magnetic field lines. With this property, the magnetic particles in a carrier fluid can be made convection-controllable agents. Regulation of convection is needed in few applications like thermoacoustic engine and pulse tube cryocoolers and hence the study of ferroconvection merits special treatment. Studies on chaotic motion in the ferroconvection problem are rather limited. The results of problems like the present work provide a guidance on the adequate number of modes required for studying the onset of convection as well as on the onset of chaos/hyper-chaos in ferrofluid-based thermoconvective systems. Important conclusions from the study are:

(i) Minimal-mode truncated Fourier solution is not the only optimal mode as far as regular convective motion is concerned.
(ii) Existence of mildly chaotic/nearly periodic points is a consequence of using minimal modes and thus chaos and fully periodic motions are the possibilities after the regular convection motion.
(iii) Influence of the magnetic field is to advance the onset of regular convective as well as chaotic motions.
(iv) A completely different chaotic scenario when using higher modes makes the study interesting compared to that of the three modes one where we see a similar scenario to that of the classical Lorenz model but with a shift in the value of r.
(v) The unstable-state behavior of the tenth-order dynamical system for moderate Pr signifies the importance of the working fluid medium on the system.
(vi) Appearance of the hyper-chaotic state in the higher-dimensional system can be retained in the same state by turning on a magnetic field of appropriate strength.
(vii) A similar study considering effective viscosity which includes the thermo-magnetic effect is under progress.

ACKNOWLEDGMENTS

C.K. is grateful to the Universidad de Tarapacá (Chile) for supporting her research work. J.A.V. and D.L. acknowledge partial financial support from Centers of Excellence with BASAL/ANID financing (Grant No. AFB180001), CEDENNA. L.M.P. acknowledges financial support from ANID through Convocatoria Nacional Subvención a Instalación en la Academia Convocatoria Año 2021 (Grant No. SA77210040).

AUTHOR DECLARATIONS

Conflict of Interest

The authors have no conflicts to disclose.

Author Contributions

C. Kanchana: Investigation (equal); Methodology (equal); Validation (equal); Visualization (equal); Writing – original draft (equal); Writing – review & editing (equal). **J. A. Vélez:** Data curation (equal); Formal analysis (equal); Software (equal). **L. M. Pérez:** Data curation (equal); Formal analysis (equal); Software (equal). **D. Laroze:** Conceptualization (equal); Funding acquisition (equal); Project administration (equal); Supervision (equal); Validation (equal); Visualization (equal); Writing – original draft (equal); Writing – review & editing (equal). **P. G. Siddheshwar:** Conceptualization (equal); Methodology (equal); Supervision (equal); Validation (equal); Writing – original draft (equal); Writing – review & editing (equal).

DATA AVAILABILITY

The data that support the findings of this study are available from the corresponding author upon reasonable request.

REFERENCES

[1]S. U. S. Choi and J. A. Eastman "Enhancing thermal conductivity of fluids with nanoparticles," *ASME International Mechanical Engineering Congress & Exposition*, November 12–17, 1995 (ASME, 1995).
[2]H. Masuda, A. Ebata, K. Teramae, and N. Hishinuma, "Alteration of thermal conductivity and viscosity of liquid by dispersing ultra fine particles," Netsu Bussei **7**, 227–233 (1993).
[3]P. G. Siddheshwar, C. Kanchana, Y. Kakimoto, and A. Nakayama, "Steady finite-amplitude Rayleigh–Bénard convection in nanoliquids using a two-phase model: Theoretical answer to the phenomenon of enhanced heat transfer," ASME J. Heat Transfer **139**, 012402 (2017).

Published under an exclusive license by AIP Publishing

[4]C. Kanchana and Y. Zhao, "Effect of internal heat generation/absorption on Rayleigh–Bénard convection in water well-dispersed with nanoparticles or carbon nanotubes," Int. J. Heat Mass Transfer **127**, 1031–1047 (2018).
[5]C. Kanchana, Y. Zhao, and P. G. Siddheshwar, "A comparative study of individual influences of suspended multiwalled carbon nanotubes and alumina nanoparticles on Rayleigh–Bénard convection in water," Phys. Fluids **30**, 084101 (2018).
[6]R. E. Rosensweig, J. W. Nestor, and R. S. Timmins, *Ferrohydrodynamic Fluids for Direct Conversion of Heat Energy. Materials Associated with Direct Energy Conversion* (Avco Corporation, Wilmington, 1965).
[7]R. Kaiser and R. E. Rosensweig, *Study of Ferromagnetic Liquid* (National Aeronautics and Space Administration, Washington DC, 1969).
[8]M. T. Shliomis, "Magnetic fluid," Sov. Phys. Usp. **17**, 153–169 (1974).
[9]R. E. Rosensweig, *Ferrohydrodynamics* (Cambridge University Press, Cambridge, 1985).
[10]R. E. Rosensweig, *Ferrohydrodynamics* (Dover Publications, Courier Corporation, Mineola, New York, 1997).
[11]B. A. Finlayson, "Convective instability of ferromagnetic fluids," J. Fluid Mech. **40**, 753–167 (1970).
[12]L. Schwab, U. Hildebrandt, and K. Stierstadt, "Magnetic Bénard convection," J. Magn. Magn. Mater. **39**, 113–124 (1983).
[13]P. J. Stiles and M. J. Kagan, "Thermo-convective instability of a horizontal layer of ferrofluid in a strong vertical magnetic field," J. Magn. Magn. Mater. **85**, 196–198 (1990).
[14]P. J. Blennerhassett, F. Lin, and P. J. Stiles, "Heat transfer through strongly magnetized ferrofluids," Proc. Roy. Soc. London A **433**, 165–177 (1991).
[15]N. Rudraiah and G. N. Sekhar, "Convection in magnetic fluids with internal heat generation," ASME J. Heat Transfer **113**, 122–127 (1991).
[16]D. P. Lalas and S. Carmi, "Thermoconvective stability of ferrofluids," Phys. Fluids **14**, 436–437 (1971).
[17]M. D. Gupta and A. S. Gupta, "Convective instability of a layer of a ferromagnetic fluid rotating about a vertical axis," Int. J. Eng. Sci. **17**, 271–277 (1979).
[18]P. G. Siddheshwar, "Rayleigh–Bénard convection in a ferromagnetic fluid with second sound," Proceedings of Japan Soc. Of Magnetic Fluids **25**, 32–36 (1993).
[19]P. G. Siddheshwar, "Convective instability of ferromagnetic fluids bounded by fluid permeable magnetic boundaries," J. Magn. Magn. Mater. **149**, 148–150 (1995).
[20]R. Bajaj and S. K. Malik, "Pattern formation in ferrofluids," J. Magn. Magn. Mater. **149**, 158–161 (1995).
[21]R. Bajaj and S. K. Malik, "Convective instability and pattern formation in magnetic fluids," J. Math. Anal. Appl. **207**, 172–191 (1997).
[22]P. G. Siddheshwar and A. Abraham, "Effect of time-periodic boundary temperatures/body force on Rayleigh–Bénard convection in a ferromagnetic fluid," Acta Mech. **161**, 131–150 (2003).
[23]T. Y. Chong, K. L. Ho, and B. H. Ong, "Investigations of field instability of ferrofluid in hypergravity and microgravity," AIP Adv. **2**, 012138 (2012).
[24]B. Straughan, "Ferrohydrodynamic convection," in *The Energy Method, Stability, and Nonlinear Convection* (Applied Mathematical Sciences, Springer, New York, 2004).
[25]Sunil and A. Mahajan, "A nonlinear stability analysis for magnetized ferrofluid heated from below," Proc. Roy. Soc. London A **464**, 83–98 (2004).
[26]P. G. Siddheshwar, O. P. Suthar, and C. Kanchana, "Finite-amplitude ferroconvection and electro-convection in a rotating fluid," SN Appl. Sci. **1**, 1542 (2019).
[27]P. N. Kaloni and J. X. Lou, "Convective instability of magnetic fluids," Phys. Rev. E **70**, 026313 (2004).
[28]S. A. Suslov, "Thermomagnetic convection in a vertical layer of ferromagnetic fluid," Phys. Fluids **24**, 084101 (2008).
[29]P. Dey and S. A. Suslov, "Thermomagnetic instabilities in a vertical layer of ferrofluid: Nonlinear analysis away from a critical point," Fluid Dyn. Res. **48**, 061404 (2016).
[30]A. Mahajan and M. K. Sharma, "Penetrative convection in magnetic nanofluids via internal heating," Phys. Fluids **29**, 034101 (2017).
[31]A. Mahajan and H. Parashar, "Linear and weakly nonlinear stability analysis on a rotating anisotropic ferrofluid layer," Phys. Fluids **32**, 024101 (2020).
[32]A. C. Melson, G. N. Sekhar, and P. G. Siddheshwar, "Nonlinear analysis of effect of rigid body rotation on ferroconvection," ASME J. Heat Transfer **142**, 061802 (2020).
[33]L. M. Pérez, J. Bragard, H. L. Mancini, P. Díaz, D. Laroze, and H. Pleiner, "Magneto-viscous effect on thermal convection thresholds in an Oldroyd magnetic fluid," J. Magn. Magn. Mater. **444**, 432 (2017).
[34]D. Laroze and H. Pleiner, "Thermal convection in a nonlinear non-Newtonian magnetic fluid," Commun. Nonlinear Sci. Numer. Simul. **26**, 167 (2015).
[35]L. M. Pérez, D. Laroze, P. Diaz, J. Martinez-Mardones, and H. L. Mancini, "Rotating convection in a viscoelastic magnetic fluid," Journal of Magnetism Magnetic Materials **364**, 98 (2014).
[36]D. Laroze, J. Martinez-Mardones, and H. Pleiner, "Bénard–Marangoni instability in a viscoelastic ferrofluid," Eur. Phys. J. Spec. Topic **219**, 71 (2013).
[37]L. M. Pérez, J. Bragard, D. Laroze, J. Martinez-Mardones, and H. Pleiner, "Thermal convection thresholds in an Oldroyd magnetic fluid," J. Magn. Magn. Mater. **323**, 691 (2011).
[38]D. Laroze, J. Martinez-Mardones, L. M. Pérez, and R. G. Rojas, "Stationary thermal convection in a viscoelastic ferrofluid," J. Magn. Magn. Mater. **322**, 3576 (2010).
[39]D. Laroze, J. Martinez-Mardones, and L. M. Pérez, "Amplitude equation for stationary convection in a viscoelastic ferrofluid," Int. J. Bifurcat. Chaos **20**, 235 (2010).
[40]D. Laroze, J. Martinez-Mardones, L. M. Pérez, and Y. Rameshwar, "Amplitude equation for stationary convection in a rotating binary ferrofluid," Int. J. Bifurcat. Chaos **19**, 2755–2764 (2009).
[41]D. Laroze, J. Martinez-Mardones, J. Bragard, and P. Vargas, "Convection in rotating binary ferrofluid," Phys. A **371**, 46 (2006).
[42]E. N. Lorenz, "Deterministic nonperiodic flow," J. Atmos. Sci. **20**, 130–141 (1963).
[43]M. Giglio, S. Musazzi, and U. Perini, "Transition to chaotic behavior via a reproducible sequence of period-doubling bifurcations," Phys. Rev. Lett. **47**, 243–246 (1981).
[44]J. B. McLaughlin and S. A. Orszag, "Transition from periodic to chaotic thermal convection," J. Fluid Mech. **122**, 123–142 (1982).
[45]W. Decker, W. Pesch, and A. Weber, "Spiral defect chaos in Rayleigh–Bénard convection," Phys. Rev. Lett. **75**, 648–651 (1994).
[46]H. Ishida, S. Kawase, and H. Kimoto, "The second largest Lyapunov exponent and transition to chaos of natural convection in a rectangular cavity," Int. J. Heat Mass Transfer **49**, 5035–5048 (2006).
[47]J. C. Sprott, "Simplifications of the Lorenz attractor," Nonlinear Dyn. Psychol. Life Sci. **13**, 271–278 (2009).
[48]R. Barrio and S. Serrano, "Bounds for the chaotic region in the Lorenz model," Phys. D **238**, 1615–1624 (2009).
[49]P. Vadasz, "Analytical prediction of the transition to chaos in Lorenz equations," Appl. Math. Lett. **23**, 503–507 (2010).
[50]D. Puigjaner, J. Herrero, C. Simó, and F. Giralt, "From steady solutions to chaotic flows in a Rayleigh–Bénard problem at moderate Rayleigh numbers," Phys. D **240**, 920–934 (2011).
[51]X. Wang and G. Chen, "Constructing a chaotic system with any number of equilibria," Nonlinear Dyn. **71**, 429–436 (2013).
[52]S. Paul and M. K. Varma, "Bifurcation analysis of the flow patterns in two dimensional Rayleigh–Bénard convection," Int. J. Bifurcat. Chaos **22**, 1230018 (2012).
[53]C. Sparrow, *The Lorenz Equations: Bifurcations, Chaos, and Strange Attractors* (Springer Verlag, New York, 1982).
[54]A. J. Lichtenberg and M. A. Lieberman, *Regular and Chaotic Dynamics*, 2nd ed. (Springer-Verlag, New York, 1992).
[55]S. H. Strogatz, *Nonlinear Dynamics and Chaos* (Westview Press, MA, 1994).
[56]R. C. Hilborn, *Chaos and Nonlinear Dynamics* (Oxford University Press, 1999).
[57]A. A. Bozhko and G. F. Putin, "Heat transfer and flow patterns in ferrofluid convection," Magnetohydrodynamics **39**, 147–169 (2003).
[58]D. Laroze, P. G. Siddheshwar, and H. Pleiner, "Chaotic convection in a ferrofluid," Commun. Nonlinear Sci. Numer. Simul. **18**, 2436–2447 (2013).
[59]M. Clerc, P. Coullet, and E. Tirapegui, "Lorenz bifurcation: Instabilities in quasireversible systems," Phys. Rev. Lett. **83**, 3820–3823 (1999).

Published under an exclusive license by AIP Publishing

[60]B. Saltzman, "Finite amplitude free convection as an initial value problem-I," J. Atmos. Sci. **19**, 329–341 (1962).
[61]D. Roy and Z. E. Musielak, "Generalized Lorenz models and their routes to chaos. I. Energy-conserving vertical mode truncations," Chaos Solitons Fracals **32**, 1038–1052 (2007).
[62]D. Roy and Z. E. Musielak, "Generalized Lorenz models and their routes to chaos. II. Energy-conserving vertical mode truncations," Chaos Solitons Fracals **31**, 747–756 (2007).
[63]D. E. Musielak, Z. E. Musielak, and K. S. Kennamer, "The onset of chaos in nonlinear dynamical systems determined with a new fractal technique," Fractals **13**, 19–31 (2004).
[64]Z. E. Musielak and D. E. Musielak, "High-dimensional chaos in dissipative and driven dynamical system," Int. J. Bifurcat. Chaos **19**, 2823–2869 (2009).
[65]B. Shen, "Nonlinear feedback in a five-dimensional Lorenz model," J. Atmos. Sci. **71**, 1701–1723 (2014).
[66]K. R. Rajagopal, M. Ruzicka, and A. R. Srinivasa, "On the Oberbeck–Boussinesq approximation," Math. Models Methods Appl. Sci. **8**, 1157–1167 (1996).
[67]S. Chandrasekhar, *Hydrodynamic and Hydromagnetic Stability* (Clarendon Press, Oxford, 1961).
[68]P. Bergé, Y. Pomeau, and C. Vidal, *Order Within Chaos: Towards a Deterministic Approach to Turbulence* (John Wiley & Sons, New York, 1987).
[69]C. Kanchana, Y. Su, and Y. Zhao, "Regular and chaotic Rayleigh–Bénard convective motions in methanol and water," Commun. Nonlinear Sci. Numer. Simul. **83**, 105129 (2020).
[70]E. N. Lorenz, "The local structure of a chaotic attractor in four dimensions," Phys. D **13**, 90–104 (1984).
[71]P. G. Siddheshwar and D. Radhakrishna, "Linear and nonlinear electroconvection under AC electric field," Communication in Nonlinear Science and Numerical Simulation **17**, 2883–2895 (2012).
[72]J. P. Gollub and S. V. Benson, "Many routes to turbulent convection," J. Fluid Mech. **100**, 449 (1980).
[73]J. H. Curry, J. R. Herring, J. Loncaric, and S. A. Orszag, "Order and disorder in two- and three-dimensional Bénard convection," J. Fluid Mech. **147**, 1 (1984).
[74]H. Yahata, "Transition to turbulence in the Rayleigh–Beńard convection," Progr. Theor. Phys. **68**, 1070 (1982).
[75]H. Yahata, "Period-doubling cascade in the Rayleigh–Bénard convection," Progr. Theoret. Phys. **69**, 1802 (1983).
[76]A. Glukhovskii and F. Dolzhanskii, "Three-component geostrophic models of convection in a rotating fluid," Akademiia Nauk SSSR Fizika Atmosfery i Okeana (Published by The Russian Academy of Sciences ISSN: 0002-3515) **16**, 451–162 (1980).
[77]I. Garashchuk, N. Kudryashov, and D. Sinelshchikov, "On the analytical properties and some exact solutions of the Glukhovsky–Dolzhansky system," J. Phys.: Conf. Ser. **788**, 012013 (2017).
[78]N. Kuznetsov, G. Leonov, and T. Mokaev, "Hidden attractor in the Rabinovich system," arXiv **1504**, 04723 (2015).
[79]G. Leonov, N. Kuznetsov, and T. Mokaev, "Homoclinic orbits, and self-excited and hidden attractors in a Lorenz-like system describing convective fluid motion," Eur. Phys. J. Spec. Topic **224**, 1421–1458 (2015).
[80]A. Wolf, J. B. Swift, H. L. Swinney, and J. A. Vastano, "Determining Lyapunov exponents from a time series," Phys. D **16**, 285–317 (1985).
[81]J. C. Sprott, *Chaos and Time-Series Analysis* (Oxford University Press, 2003).
[82]J. A. C. Gallas, "The structure of infinite periodic and chaotic hub cascades in phase diagrams of simple autonomous flows," Int. J. Bifurcat. Chaos **20**, 197–211 (2010).
[83]L. M. Pérez, J. Bragard, H. L. Mancini, J. A. C. Gallas, A. M. Cabanas, O. J. Suarez, and D. Laroze, "Effect of anisotropies on the magnetization dynamics," Netw. Heterog. Media **10**, 209–221 (2015).
[84]J. A. Vélez, J. Bragard, L. M. Pérez, A. M. Cabanas, O. J. Suarez, D. Laroze, and H. L. Mancini, "Periodicity characterization of the nonlinear magnetization dynamics," Chaos **30**, 093112 (2020).
[85]A. Pikovsky and A. Politi, *Lyapunov Exponents: A Tool to Explore Complex Dynamics* (Cambridge University Press, 2016).
[86]P. C. Rech, S. Dhua, and N. C. Pati, "Multistability and bubbling route to chaos in a deterministic model for geomagnetic field reversals," Int. J. Bifurcat. Chaos **29**, 1930034 (2019).
[87]J. A. Gallas, "Stability diagrams for a memristor oscillator," Eur. Phys. J. Spec. Topic **228**, 2081 (2019), and references therein.
[88]R. Barrio, M. Á. Martínez, S. Serrano, and D. Wilczak, "When chaos meets hyperchaos: 4D Rössler model," Phys. Lett. A **379**, 2300–2305 (2015).
[89]P. G. Siddheshwar and P. S. Titus, "Nonlinear Rayleigh–Bénard convection with variable heat source," ASME J. Heat Transfer **135**, 122502 (2013).
[90]C. D. Li, X. F. Liao, and K. Wong, "Lag synchronization of hyperchaos with application to secure communications," Chaos, Solitons Fractals **23**, 183–193 (2005).
[91]K. M. Cuomo and A. V. Oppenheim, Circuit implementation of synchronizing chaos with applications to communications," Phys. Rev. Lett. **71**, 65–68 (1993).

Published under an exclusive license by AIP Publishing